Received: 31 January 2025 | Revised: 18 December 2025 | Accepted: 24 December 2025

DOI: 10.1002/esp.70246

RESEARCH ARTICLE

ESPL WILEY

Palaeoglacier reconstruction and dynamics of Cordillera Vilcanota in the tropical high Peruvian Andes

Bethan Davies[1] | Tom Gribbin[2,3] | Owen King[1] | Tom Matthews[4] | Jan R. Baiker[5] | Wouter Buytaert[6] | Jonathan Carrivick[7] | Fabian Drenkhan[8,9] | Juan-Luis García[10] | Nilton Montoya[11] | L. Baker Perry[12,13] | Jeremy Ely[14]

[1]School of Geography, Politics and Sociology, Newcastle University, Newcastle-upon-Tyne, UK

[2]British Geological Survey, Environmental Science Centre, Keyworth, UK

[3]School of Geography, Earth and Environmental Sciences, University of Birmingham, Edgebaston, Birmingham, UK

[4]Department of Geography, Kings College London, London, UK

[5]ACEMAA (Asociación para la Conservación y Estudio de Montañas Andinas-Amazónicas), Cuzco, Peru

[6]Imperial College London, London, UK

[7]School of Geography and water@leeds, University of Leeds, Leeds, UK

[8]Geography and Environment, Department of Humanities, Pontificia Universidad Católica del Perú, Lima, Peru

[9]Grupo de Glaciología y Ecohidrología de Montañas Andinas (GEMS), Institute for Nature, Earth and Energy (INTE), Pontificia Universidad Católica del Perú, Lima, Peru

[10]Instituto de Geografía, Facultad de Historia, Geografia y Ciencia Política, Pontificia Universidad Católica de Chile, Santiago, Chile

[11]Universidad Nacional de San Antonio Abad del Cusco, Cusco, Peru

[12]Department of Geography, University of Nevada, Reno, Reno, NV, USA

[13]Research Institute for Environment, Energy, & Economics, Appalachian State University, Boone, NC, USA

[14]School of Geography and Planning, The University of Sheffield, Sheffield, UK

Correspondence
Bethan Davies, School of Geography, Politics and Sociology, Newcastle University, Newcastle-upon-Tyne, UK.
Email: bethan.davies@newcastle.ac.uk

Funding information
Natural Environment Research Council, Grant/Award Numbers: NE/X004031/1, NE/S007350/1

Abstract

Tropical glaciers are important indicators of climate change, provide freshwater resources for downstream communities, and form an important component of the hydrological cycle. Understanding the dynamics and patterns of behaviour of tropical palaeoglaciers is important for interpreting their sensitivities and vulnerabilities. Glacier advances in the high tropical Peruvian Andes occurred multiple times during the last glacial cycle and Holocene, leaving complex geomorphological evidence on the landscape. The substantial topographic, geological and climatic variability in this region leads to high geomorphic diversity. However, few detailed geomorphological studies have been conducted to date, leading to considerable uncertainty in the behaviours and drivers of tropical palaeoglaciers. Here, we provide a detailed geomorphological analysis of the Cordillera Vilcanota, Cusco region, southern Peru (71°W, 13.7°S), and use morphostratigraphic principles to reconstruct the former maximum icefield extent and palaeoglacier advances. Across this domain, we mapped ~23,000 features encompassing five key environments: glacier, subglacial, ice-marginal, fluvial and lacustrine. The mapped features show evidence of both modern-day polythermal and temperate ice margins, with low meltwater volumes leading to small-scale glaciofluvial landform formation. However, larger moraines, beyond those well-dated to the Younger Dryas and Antarctic Cold Reversal, assumed to represent Last Glacial Maximum and earlier advances, suggest that conditions were temperate and drained by more substantial rivers, with coupled flow of ice and till, and evidence of subglacial scouring, drumlin formation and the deposition of substantial moraines and large palaeosandar. Our reconstructed maximum icefield covers 2,660 km^2 and was drained by multiple topographically constrained ice lobes across the region. In the north, these ice lobes reached an elevation of 3,500 m asl, but were limited to above 4,500 m asl in the south, likely reflecting the dominant moisture sources. Our geomorphological mapping reveals seven clear ice margins, morphostratigraphically correlated across the study region, reflecting at least seven palaeoglacier advances during the last glacial cycle, including the Late Glacial period and the Holocene.

KEYWORDS
Andes, Geomorphology, Glacier, Peru

1 | INTRODUCTION

In the Andean Tropics from 11°N to 17°S, glaciers are restricted to very high altitudes, with highly seasonal precipitation patterns, year-round melt and high solar radiation. This high solar radiation means that snow falling off-glacier melts very quickly. The tropical glaciers in the Andes are, as a result, very important for meltwater, especially in the dry season (Buytaert et al., 2017; Soruco et al., 2015), and sustain important hydropower schemes and irrigation (Immerzeel et al., 2020). They are sensitive indicators of climate change (Licciardi et al., 2009), with accelerating glacier thinning and recession; Andean glaciers are thinning by an average of -0.69 m y^{-1}, 35% faster than the global average (-0.46 m y^{-1}) (Hugonnet et al., 2021). This makes moraine sequences important palaeoclimatic indicators. Accurate documentation of past glacier fluctuations here is important to better understand the climatic processes, thresholds and drivers of mass-balance sensitivities. These insights can help understand mechanisms for natural climate variability in the Tropical Andes.

Glacial advances are recognised in the tropical Peruvian Andes during the global Last Glacial Maximum (gLGM; c. 23 to 19 ka; Hughes et al. (2013)), Antarctic Cold Reversal (ACR; 14.7 to 13.0 ka; Pedro et al. (2016)) and Younger Dryas (YD; 12.9 to 11.7 ka; Rasmussen et al. (2006)), as well as during the 'Little Ice Age' (LIA) chronozone (1,250 to 1860 CE; Wanner et al. (2022)) (Carrivick et al., 2024; Glasser et al., 2009a; Jomelli et al., 2011, 2014, 2017; Kelly et al., 2015; Lee et al., 2022; Sagredo et al., 2016), leaving a distinctive glaciated landscape. However, the resultant geomorphology, glacier dynamics and thermal regimes under different palaeoclimates and atmospheric CO_2 concentrations are poorly understood in the tropical Andes, with high spatial and topographic variability across the tropical Andes and few detailed glacial geomorphological studies available (Iturrizaga, 2018; Małecki et al., 2018; Narro Pérez et al., 2023; Rabatel et al., 2006). Understanding the dynamics and patterns of behaviour here is important for interpreting contemporary tropical glacier drivers, sensitivities and vulnerabilities.

In this study, we seek to map and understand the significant scars and marks left on the landscape in the high Peruvian Andes and use morphostratigraphic principles to reconstruct palaeoglacier advances. We use these data to provide an insight into past glacier behaviour, which is critical to understand past and current glacier-climate interactions and offers empirical data for model-data comparisons. This research, therefore, aims to use a geomorphological approach to understand the evolving relationships between glaciers, geomorphology and climate. Detailed geomorphological maps are critical for establishing future cosmogenic chronologies and for understanding the relationship between glaciers, glacial geomorphology, hydrology and the high-altitude wetlands known locally as *bofedales* (see Davies et al., n.d.).

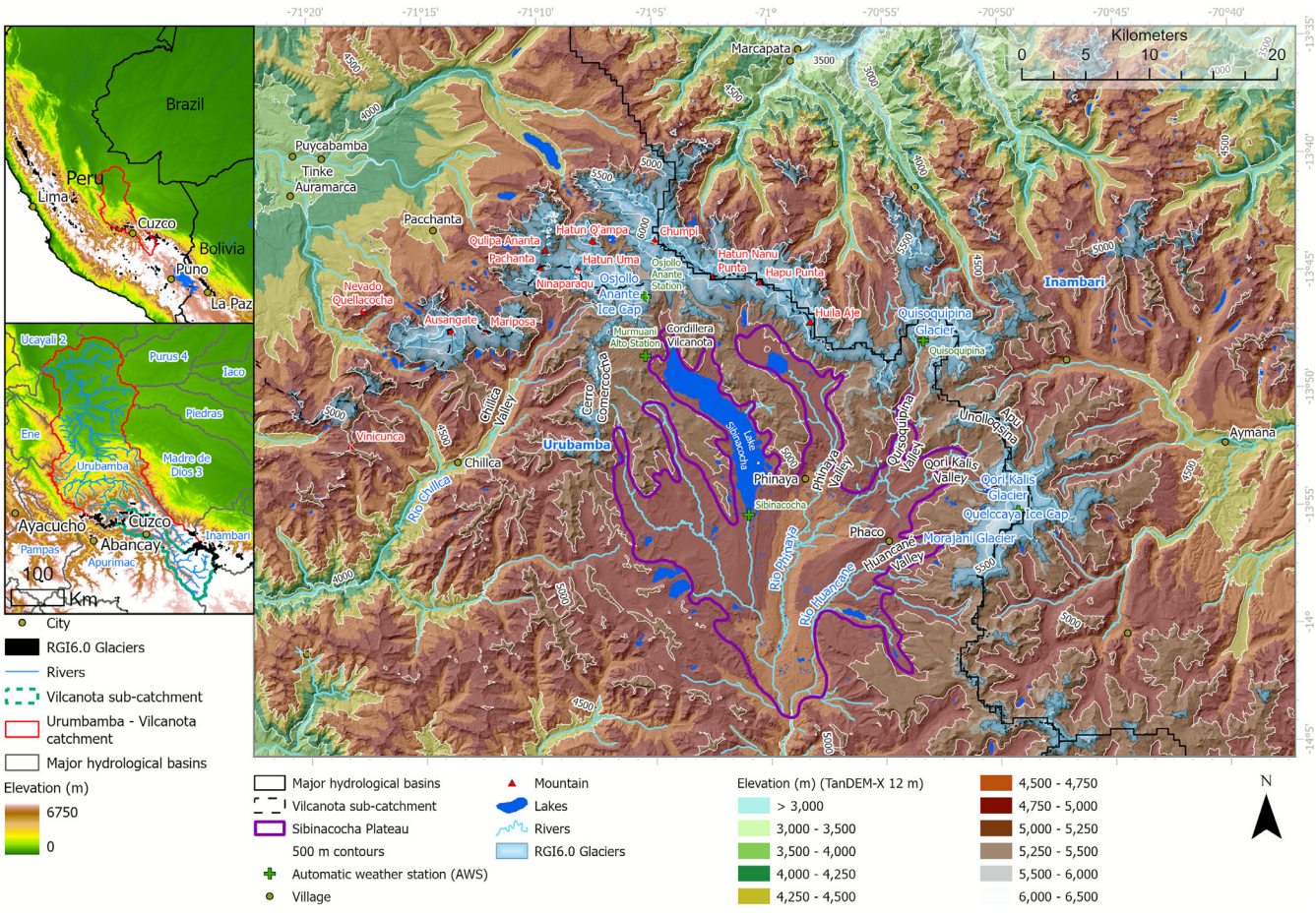

FIGURE 1 Study domain: Cordillera Vilcanota in the high Peruvian Andes. A. The Urubamba-Vilcanota hydrological catchment within Peru. B: The Vilcanota catchment within the broader Vilcanota-Urubamba catchment and significant cities. C: The study domain, along with the Sibinacocha Plateau (purple). Hydrological basins and basin-wide rivers from Hydrosheds (Lehner et al., 2008). The glaciers and rivers here are tributaries to Río Vilcanota. Elevation from TanDEM-X (12 m).

2 | STUDY AREA

2.1 | Topography and geology

Cordillera Vilcanota (71°W, 13.7°S) lies in the Cuzco region of Peru (Figure 1A,B), straddling the Vilcanota and Inambari hydrological catchments. The Río Vilcanota sub-catchment of the Vilcanota-Urubamba hydrological basin lies south of the ice divide (Figure 1). Both of these catchments drain towards the Amazon River basin (Drenkhan et al., 2015). The Vilcanota-Urubamba River and its tributaries (Figure 1) supply the rural pastoralist Quechua communities and urban areas with water for multiple activities, including irrigation for local and export agriculture, livestock, domestic use, hydropower and tourism (Drenkhan et al., 2019; Muñoz et al., 2024; Perry et al., 2014; Salzmann et al., 2013; Vergara et al., 2007). Lake Sibinacocha is dammed at the southern margin and used for hydropower generation at the far outlet of the Vilcanota-Urubamba basin, where the important Machu Picchu and Santa Teresa hydroelectric plants are located (Bello et al., 2023).

Cordillera Vilcanota includes the Osjollo Ice cap with Mt Hatun Uma (6,093 m), Nevado Ausangate (6,384 m) and Mt Chumpi (6,106 m) (Figure 1C), which are all drained by tributaries of Río Vilcanota. These glacierised peaks bear the second largest coverage of mountain glacier ice in Peru after Cordillera Blanca (INAIGEM, 2018, 2023). This range comprises resistant igneous granodiorite to quartz monazite intrusions. Between the glacierised mountain peaks, for example, near the peaks of Huila Aje, Chumpi or Hatun Nanu Punta lie wide, over-deepened parabolic valleys, often with lakes along their valley floor. Quelccaya Ice Cap (70.8°W, 13.9°S; 38.8 km^2 in the INAIGEM 2020 inventory [INAIGEM, 2023]), at the southeastern margin of the Cordillera Vilcanota, is the world's second-largest tropical ice cap after Coropuna Ice Cap in Cordillera Ampato, southern Peru (72°38'W, 15°33'S; 42.4 km^2 in the INAIGEM 2020 inventory) (INAIGEM, 2023; Kochtitzky et al., 2018). Quelccaya Ice Cap rests on a raised ignimbrite plateau.

These aforementioned glacierised uplands arc around the 'Sibinacocha Plateau' (Figure 1C), an intramountainous depression, which bears numerous lakes (such as the 15 km long Lake Sibinacocha) and wetlands. We here define the Sibinacocha Plateau as the area of low slope between 4,800 and 5,200 m asl (mean 4,875 m asl) (Figure 1C). The Sibinacocha Plateau south of the Cordillera is some 359 km^2, with regional slopes generally below 5°. It is some 25 km wide (west to east) and 30 km long (north–south).

The Sibinacocha Plateau comprises a range of (meta)sedimentary facies, including slates and Early Palaeozoic and Cretaceous sedimentary strata, within which there is an abundance of Triassic, Neogene and Jurassic plutonic intrusive rocks and Permian–Triassic volcanics (Audebaud, 1973; INGEMMET, 2025). These geological intrusions and plateaux stand proud above the surrounding landscape. During past glacial periods, the Quelccaya Ice Cap and the Cordillera Vilcanota icefield combined and interacted to form a large icefield on this plateau (Mercer & Palacios, 1977), which separated in the Early Holocene (Mark et al., 2002). As a result, the plateau is dominated by glacial landforms, including sequences of nested lateral and terminal moraines.

The Sibinacocha Plateau in the centre of the study domain is dissected by several main river valleys that drain from the high mountains (Figure 1C). The valley draining southwards from Mt. Chumpi is occupied by Lake Sibinacocha. A weather station is located at the dam at the foot of the lake (4,985 m asl). Moving eastwards, the Phinaya Valley with Río Phinaya drains southward from Mt. Hatun Nanu Punta and Hapu Punta, with the village of Phinaya located some 14 km down-valley of the peaks. The Phinaya Valley, occupied by Río Phinaya, extends to the southern margin of the Sibinacocha Plateau, where it joins Río Huancané. The next major valley is the Quisoquipina Valley, with the Suyuparina and Quisoquipina glaciers at the head of the valley. A weather station is located off-ice at the head of the Quisoquipina valley (5,180 m asl). Quisoquipina Valley joins Phinaya Valley within the Sibinacocha Plateau.

The Qori Kalis valley, with Río Qori Kalis, drains from the Quelccaya Ice Cap into the Río Phinaya valley. Other significant valleys draining from Quelccaya towards Río Phinaya include the smaller Challpacocha Valley and the Huancané Valley, occupied by Río Huancané (Figure 1C). Quelccaya Weather Station is located at 5610 m asl on the plateau of Quelccaya Ice Cap. Río Huancané, Río Phinaya and Río Chillca eventually join Río Vilcanota, some distance down-valley of the study domain.

The lowest elevations in the domain, below 3,500 m asl, occur north of the cordillera (Figure 1C). Away from the ice masses, the south-western and north-eastern corners of the study domain are dominated by steeply incised fluvial geomorphology, with no present-day glaciers and only small-scale evidence of smaller mountain palaeoglaciers.

In the western part of the study domain, the Chillca Valley, occupied by Río Chillca, drains southwards from Osjolla Anante Ice Cap, with the high peaks of Pachanta (5,950 m) and Hatun Uma (6,093 m) at the head of the valley. The Ausangate massif lies west of the Chillca Valley. The village of Chillca lies mid-way down-valley.

2.2 | Climate and glaciers

Cordillera Vilcanota lies in the wet outer tropics. This region is characterised by two distinct seasons, driven by the South American Monsoon; the warm and wet season in the austral summer, with the majority of the precipitation (October to April); and the dry and cold season in the austral winter (May to September) (Espinoza et al., 2020; Perry et al., 2014; Sagredo & Lowell, 2012) (Figure 2). Glacial meltwater sustains the water supply downstream, especially during the dry season (Bradley et al., 2006; Buytaert et al., 2017; Drenkhan et al., 2019; Gribbin et al., 2024; Schauwecker et al., 2014; Vergara et al., 2007). The low latitude and high elevation here combine to drive some of the highest levels of insolation anywhere on earth (Cordero et al., 2023). Air temperatures are accordingly high for the elevation, with the regional mean annual 0°C isotherm located slightly above 5,000 m asl (Schauwecker et al., 2017) (Figure 2). Air temperature and insolation both reach minimum values in the dry season (Figure 2). During the wet season, enhanced cloud cover reduces solar heating of the boundary layer, resulting in a relatively subtle amplitude of temperature seasonality. The enhanced atmospheric moisture content in the wet season also acts to decrease the absolute value of the lapse rate due to latent heat release, meaning that the amplitude of temperature seasonality increases with altitude (Fyffe et al., 2021).

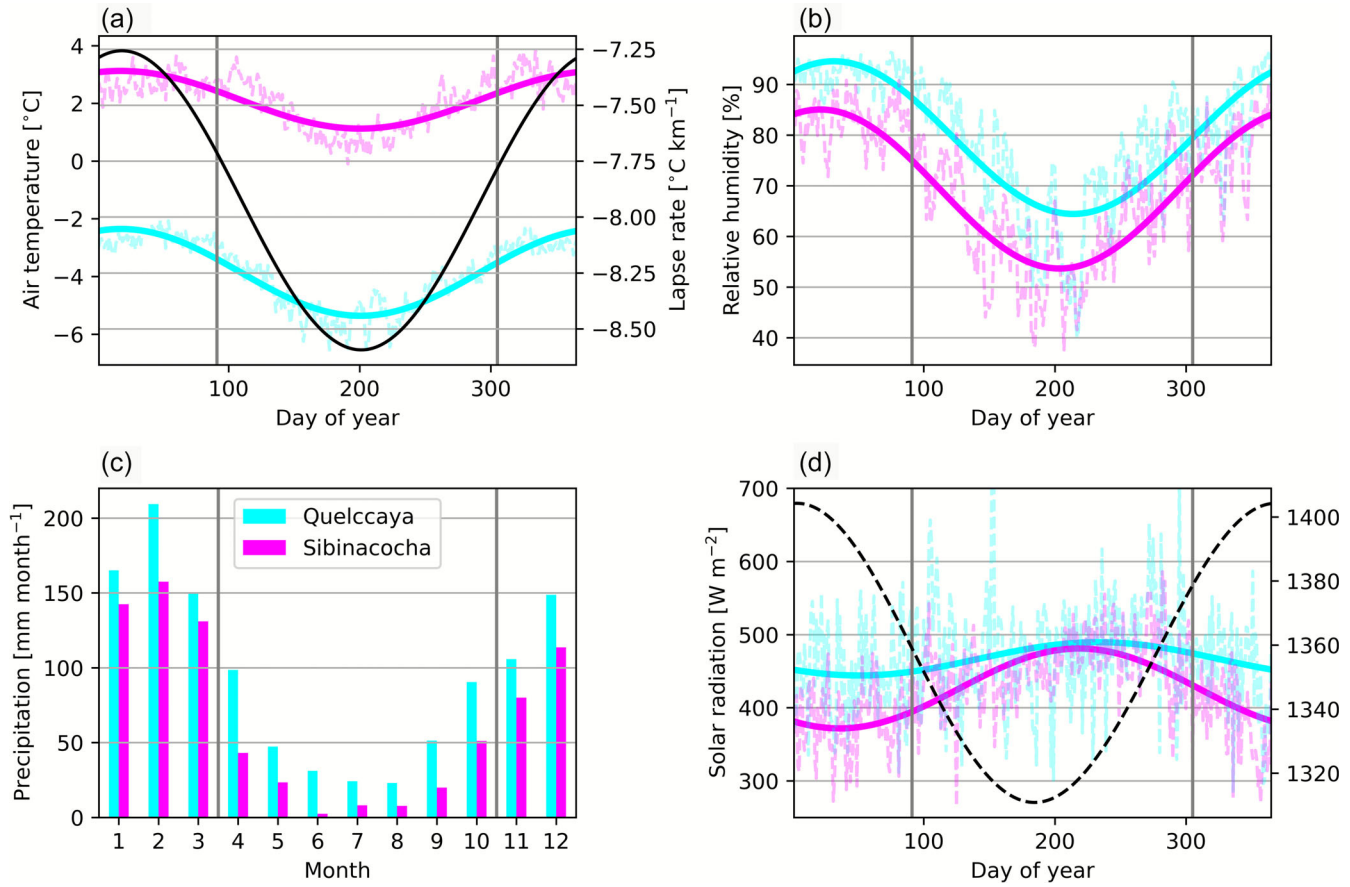

FIGURE 2 Climatology of the Cordillera Vilcanota, from two automatic weather stations: Quelccaya weather station at the top of Quelccaya Ice Cap (5,650 m) and Lake Sibinacocha weather station (4,895 m) (see Figure 1). In all panels, the vertical grey lines separate the dry season (middle) from the wet season (ends). Dashed coloured lines are the day-of-year means, and the solid coloured lines are the first harmonic (best fitting cosine wave with a period of 365.25 days). A: mean daily temperatures at Sibinacocha and Quelccaya summit. The black line represents the lapse rate. B: Relative humidity for each weather station for each day of the year. C: Mean monthly precipitation for each weather station. D: Solar radiation at the top of Earth's atmosphere for both weather stations. Note that solar radiation peaks in the dry season. The black dashed line shows the potential (top of atmosphere) shortwave radiation (at solar noon). Right-hand axis: also W m^{-2}. Data sources: (Birkel et al., 2022; Perry et al., 2017). The location of AWS is shown in Figure 1.

Precipitation events are mainly associated with backward air trajectories originating from the north and northwest. The major river valleys are the main way in which moisture is delivered to the Vilcanota (Endries et al., 2018; Junquas et al., 2018). The daily precipitation cycle is bimodal, with convective precipitation events in general most frequent in the afternoon (Endries et al., 2018), with significantly large-scale stratiform precipitation associated with airstreams arriving from the Amazon occurring more often at night (Perry et al., 2014, 2017). The coincidence with lower nighttime air temperatures makes these nocturnal precipitation events important contributors to high-elevation snowfall and hence accumulation across the glacier surface.

The seasonality in shortwave radiation, temperature, humidity and precipitation (Figure 2) together modulate glacier surface energy balances in the Cordillera Vilcanota. Net shortwave heating, the largest energy flux, peaks in the dry season (Figure 2D) despite the lower potential insolation at this time of year, due to lower cloud cover and reduced albedo (from less frequent snowfall events) (Fyffe et al., 2021; Kronenberg et al., 2016). However, the increase in downwelling longwave radiation and latent heat flux, from a warmer, moister atmosphere, more than offsets the decline in net shortwave heating so that melt energy peaks in the wet season (Fyffe et al., 2021). Sublimation, driven by high levels of insolation and low specific humidity, is also an important mechanism of mass loss in the dry season, especially at higher elevations (Fyffe et al., 2021). Therefore, ablation occurs in both the wet and dry seasons, but peaks in the wet season from September to January at the Quisoquipina Glacier weather station (Fyffe et al., 2021). Black carbon deposition on glacier tongues, particularly during the dry season, is altering the local energy balance, leading to enhanced glacial melting. This black carbon originates from down-valley urban activities and vegetation burning (Bonilla et al., 2023; Gilardoni et al., 2022; INAIGEM, 2023).

The tropical glaciers of the Cordillera Vilcanota include various glacier types, including ice caps and mountain glaciers with reduced glacier tongues. Periglacial features such as rock glaciers are also present. Steep mountain glaciers terminate at 4700 to 5,000 m asl (Salzmann et al., 2013), with equilibrium line altitudes (ELAs) at 5105 to 5,275 m asl (Mark et al., 2002). The glaciers are up to 270 m thick, but many have a maximum ice thickness of under 100 m (Millan et al., 2022). These mountain glaciers contrast with the low-slope Quelccaya Ice Cap, which reaches maximum thicknesses of nearly 400 m (ibid.). Across the entire Cordillera Vilcanota, the INAIGEM 2020 inventory noted 58 rock glaciers (1.7 km^2) (INAIGEM, 2023). Glaciers here are thinning, losing 3.18 ± 0.44 Gt of ice from 2000 to 2020 (Taylor et al., 2022). Total glacier area here shrank by 51% from

1962 to 2020 (0.9% a^{-1}) (INAIGEM, 2023). Quelccaya Ice Cap thinned by an average of −0.37 m a^{-1} from 2010 to 2020 (data from Hugonnet et al., 2021, clipped to 2022 glacier extent). Suyuparina and Quisoquipina glaciers thinned at a glacier-averaged rate of −0.92 and −0.42 m a^{-1}, respectively (2010–2020) (Hugonnet et al., 2021). Across the study domain, the mean of the glacier-averaged rate of thinning is −0.53 m a^{-1}. The fastest-thinning glaciers are fragmented tongues and isolated glacierets on the periphery of the range.

2.3 | Palaeoclimate in the Tropical Andes

Palaeoclimate records spanning the length of the last Glaciation (MIS 2–4) and Holocene (MIS 1) are sparse. Tropical ice core records from Peru indicate that the tropical Atlantic was 5–6°C cooler than today during the global Late Glacial Maximum at 23–19 ka (Hughes et al., 2013; Thompson, 2000; Thompson et al., 2017). Post-dating this, the Antarctic Cold Reversal (ACR) is a cooling event recognised in Antarctic ice cores, from 14.7–13 ka (Pedro et al., 2016). Andean climate variations captured in a sediment core from Laguna Llaviucu, Ecuador, indicate the Last Glacial Maximum was followed by warming, and then a ~ 1.5°C cold reversal coincident with the Antarctic Cold Reversal (ACR) at ~14.4 cal. ka BP (Zhao et al., 2024). A cool, dry climate during the Younger Dryas period is recorded in Lake Compuerta (3,950 m elevation) in the western Cordillera of the Peruvian Andes (Weng et al., 2006). Cooling during the Younger Dryas is also evident in ice cores from Huascarán, north-central Andes of Peru (Thompson, 2000).

Ice core records indicate that the period from 8,400 to 5,200 years before present was the warmest Holocene interval (Thompson et al., 2017). A warm-dry event from 9,500 to 7,300 cal. yr BP is also recorded in Laguna do Cochos, northern Peru (Bush et al., 2005). During this warm period, glaciers retreated, with Quelccaya Ice Cap having an extent similar to present from 7,000 to 5,200 years before present (Buffen et al., 2009), and possibly smaller than present (Vickers et al., 2021). The climate then cooled, culminating in a Little Ice age, 500–200 years ago (Thompson, 2000; Thompson et al., 2013, 2017). Warming in recent decades is unusual in the Peruvian tropics in the last 2000 years, when compared with ice core records from Quelccaya Ice Cap (Thompson et al., 2006). Annual dry seasons remain identifiable in ice cores (May–October) (Thompson, 2000).

2.4 | Palaeoglacier fluctuations in the Tropical Andes

Tropical glacier advances in the Andes have typically tracked global ice volume changes (Rodbell et al., 2022). During the last glacial cycle, glacier advances were synchronous with changes in regional monsoon strength, linked to temperature changes recorded in Greenlandic ice cores, indicating interhemispheric connections. The timing of the local Last Glacial Maximum (LLGM) in Peru is poorly constrained, with estimates ranging from 32 to 18 ka (Mark et al., 2017; Palacios et al., 2020). Smith et al. (2005a) argue that in Peru and Bolivia, glaciers reached their greatest extent at ~34 ka. The LLGM in Cordillera Vilcanota is undated, but maximum-limiting radiocarbon ages around Pacchanta, north of the icefield (Figure 3A,D), suggest that the outer moraines likely date from this time, and a pre-Global Last Glacial Maximum (gLGM, the timing of the global sea level lowstand [Hughes et al., 2013]) advance is possible based on radiocarbon ages of 32 to 35 cal. ka BP (Figure 3A; (Mercer & Palacios, 1977)). Conversely, in the Cajamarca region of northern Peru, cosmogenic exposure ages from terminal moraines indicate that the glaciers during the LLGM deposited moraines at 23.5 ± 0.5 and 21.2 ± 0.8 ka (Shakun et al., 2015), before the end of the gLGM. In Cordillera Carabaya, in the Cordillera Oriental in southern Peru, terminal moraines are dated to 28.6 ± 0.4 ka, earlier in MIS 2 (Bromley et al., 2016).

Theories of an older advance that predates the gLGM (Smith et al., 2005a, 2005b; Zech et al., 2009) conflict with studies suggesting that glaciers advanced during the time of the global LGM and global sea level lowstand (Palacios et al., 2020). However, an older advance predating the global LGM has been noted in Patagonia (Davies et al., 2020) and New Zealand (Darvill et al., 2016; Eaves et al., 2016). This ambiguity impedes our ability to examine climatic circulation patterns, mechanisms and controls. After the gLGM, the structure of tropical palaeoclimate remains uncertain, with millennial-scale cooling events typically antiphased between the northern and southern hemispheres (Zhao et al., 2024).

Advances of tropical glaciers in Peru and Bolivia have been noted at 16.1 ± 1.1 kyr, during Heinrich Stadial 1 (Bromley et al., 2016; Mark et al., 2017). Glacier advances are also clearly recorded in the tropical Andes during the Antarctic Cold Reversal (Jomelli et al., 2014, 2017), with substantial moraines in sites nationwide dated to ~14.0 ka. An Antarctic Cold Reversal readvance is evident in Cordillera Vilcanota, with the Hu-IIIa moraines in the mid-Huancané valley (Figure 1C; Figure 3C) predating 14.2 cal. ka BP (Mercer & Palacios, 1977). Just in-board of this, cosmogenic nuclide ages on the Hu-III moraines in the Huancané valley have a mean exposure age of 13.5 ka (Kelly et al., 2015).

Glacier advances are also recognised in the tropical Andes during the Younger Dryas (~12.9–11.6 ka) (Kelly et al., 2015). Cosmogenic nuclide dating on boulders on moraines in Cordillera Blanca, Peru, indicated outer moraines dated to 12.4 ka, with inner moraines indicating readvances in the Holocene (10.8, 9.7 and 7.6 ka) (Glasser et al., 2009a). In Cordillera Vilcanota, cosmogenic nuclide dating on the Hu-IIa moraines in the Huancané valley, western Quelccaya (Figure 1C; Figure 3C), yielded a mean age of 11.6 ka (standard deviation of 0.45) (Kelly et al., 2015), which is in close agreement with independent radiocarbon dating (Goodman et al., 2001; Mark et al., 2002; Mercer & Palacios, 1977).

Mid-Holocene (Licciardi et al., 2009) and Late Holocene readvances are also noted across the Andes (Bromley et al., 2011; Carrivick et al., 2024; Sagredo et al., 2016). Late-Holocene advances in Cordillera Vilcanota are specifically noted in the upper Huancané Valley, with the Challpachocha I moraines yielding ages of 0.3–0.8 cal. ka BP (Mercer & Palacios, 1977) (Figure 3C). In the Qori Kalis valley, 11 ^{10}Be ages from boulders on the Qori Kalis moraines yield a mean age of 0.5 ka (standard deviation 0.1, one anomalous boulder of 5.2 ka excluded) (Stroup et al., 2014). Five boulders taken from the innermost moraines at the lake margin yield a mean ^{10}Be exposure age of 0.2 ka (standard deviation 0.01) (Figure 3C). Finally, ^{10}Be exposure ages from the Phinaya I moraines, from the Huila Aje massif (Figure 1C; Figure 3B), yield a mean age of 0.36 ka (standard deviation 0.25) (Sagredo et al., 2016).

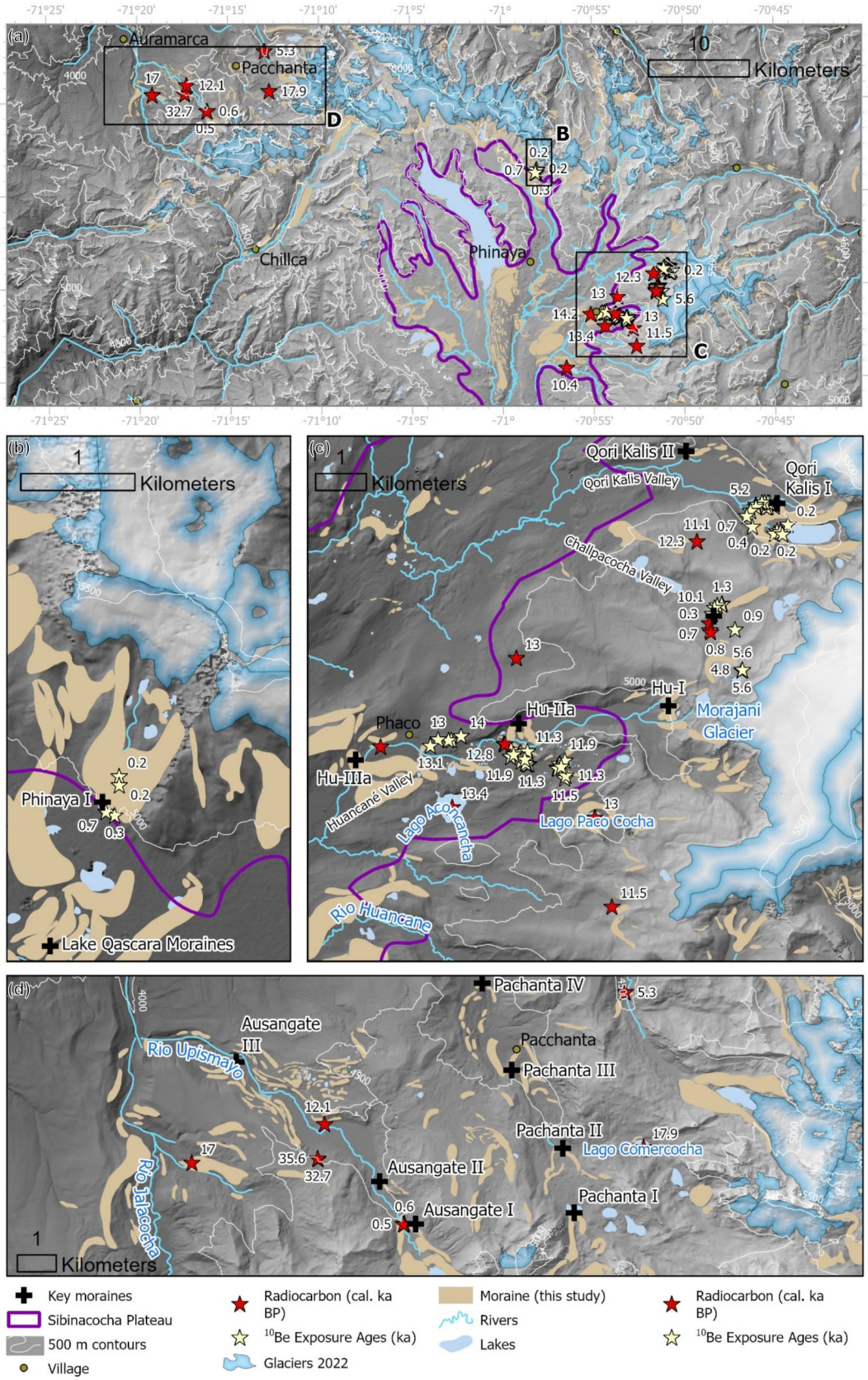

FIGURE 3 Published chronology from the Cordillera Vilcanota area. Radiocarbon ages (Goodman et al., 2001; Mark et al., 2002; Mercer & Palacios, 1977) are recalibrated using the Calib version 8.20 ^{14}C calibration programme (Stuiver & Reimer, 1993), and are presented as calibrated ages (cal. ka BP), using the IntCal20 dataset (Reimer et al., 2020). Published cosmogenic nuclide ages (Kelly et al., 2015; Sagredo et al., 2016; Stroup et al., 2014, 2015) are recalculated using the LSDn scaling scheme (Borchers et al., 2016; Lifton et al., 2014) and the global production rate (Borchers et al., 2016).

3 | METHODS

We mapped glacigenic landforms across a ~ 4,569 km^2 area (Figure 1C) of the Cordillera Vilcanota and Quelccaya region in a Geographic Information System (GIS) (ArcGIS Pro), using field surveys conducted in September 2023 and April 2024 and remote sensing from satellite imagery and digital elevation models (DEMs). Mapping was conducted through manual digitisation at a scale of 1:10,000. Landforms in the field were mapped using a handheld GPS with a documented accuracy of ± 5 m. Topographic and elevation data were derived from the TanDEM-X with 12 m spatial resolution, acquired in 2015, with hillshades (315° azimuth) and slope maps used to visualise the landscape and support landform identification. Optical satellite data utilised include the 1 m Digital Globe imagery, part of the ESRI™ World Imagery and SPOT-6 imagery (Table 1).

An uncrewed aerial vehicle (DJI Mavic 2) was used to observe landforms aerially, and to generate original orthomosaics and DEMs from aerial imagery (manually flown, camera height 30 m, camera angle 90°, 30% overlap), over the Suyuparina Glacier forefield and the Quisoquipina and Qori Kalis II Moraines. These products were generated using structure-from-motion techniques in Pix4D (Table 1), following standard procedures (Chandler et al., 2018; Le Heron et al., 2019, 2021; McCerery et al., 2024).

Landforms were identified and classified according to established glacial geomorphological criteria (Davies et al., 2022; Lee et al., 2022; Małecki et al., 2018; Martin et al., 2019; McCerery et al., 2024) (Table 2). Here, we group landforms into topographic, glacial, subglacial, ice-marginal, fluvial and lacustrine assemblages. Hydrological basins and regional-scale rivers were obtained from Hydrosheds v1 (Lehner et al., 2008). Glacier outlines were manually edited from the RGI V.6.0 (Randolph Glacier Inventory Consortium et al., 2017) to reflect glacier extent in the 2022 Sentinel image (Table 1). Outlines and ice divides were visually checked against the INAIGEM 2020 inventory (INAIGEM, 2023). Lakes were manually mapped, and the resulting shapefiles expanded on previous lake inventories that were restricted to within 3,000 m of the ice margin (Wood et al., 2021) and included lakes across the domain. The resultant lake inventory was compared manually against other published inventories (Drenkhan et al., 2019; INAIGEM, 2023; Wood et al., 2021). For both glaciers and lakes, a minimum size threshold of 2–3 pixels (200–300 m^2) was applied to avoid misclassification.

Roadside and river cuttings provided sediment exposures. Sedimentological and stratigraphical studies followed standard procedures (Evans & Benn, 2014, 2021). Clast morphology data (lithology, shape and roundness) were collected from representative facies to investigate transportation and erosion histories (following Powers, 1953; Benn, 1994, 2004, 2007; Lukas et al., 2013). Clast shape data for pebbles (8–64 mm) were plotted on a general shape ternary diagram, and C_{40} indices were calculated (Benn & Ballantyne, 1993; Sneed & Folk, 1958). 30 stones were counted in each sample.

Published cosmogenic ages (Kelly et al., 2015; Sagredo et al., 2016; Stroup et al., 2014, 2015) were collated using the ICE-D database and the literature, and are presented recalculated using the Version 3 CRONUS-Earth online exposure age calculator, to provide chronological context for mapped features. The full dataset (shapefiles and spreadsheet) is provided in the Supplementary Information. Samples are presented on maps at 0.1 ka temporal resolution, calculated using the LSDn scaling scheme (Borchers et al., 2016; Lifton et al., 2014) and the global production rate of 3.92 atoms g^{-1} yr^{-1}(Borchers et al., 2016). We also calculated ages using the Kelly et al. (2015) production rate (3.97 ± 0.09 atoms g^{-1} yr^{-1}). This leads to an average difference in age of 293 years, with a mean difference between the ages of 5.8%. This is smaller than the external age uncertainties, and certainly smaller than the resolution of the ages presented in the figures throughout the paper. Published radiocarbon ages were collated from the literature and recalibrated using the Calib version 8.20 ^{14}C calibration programme (Stuiver & Reimer, 1993), and are presented as calibrated ages (cal. ka BP), using the IntCal20 dataset (Reimer et al., 2020).

Finally, morphostratigraphic methods are used to create a reconstruction of the icefield during its maximum configuration and during retreat. Morphostratigraphic principles (cf. Boston et al., 2015; Lukas, 2006) are applied, using geomorphological variations (such as ridge crest width, slope angle, vegetation development), stratigraphic position in the valley and chronological ages where available, in the reconstruction.

TABLE 1 Data sources used in the study.

	Date acquired	Resolution	Source and Properties
Tandem-X DEM	2015	12 m	Acquisition method: Interferometric Synthetic Aperture Radar (InSAR) from the TanDEM-X satellite pair
Sentinel imagery	18.06.2022	10 m	Image ID: T18LYK_20220618T145741_B08_10m
SPOT-6 imagery	30.06.2016	1.5 m	Image ID: DS_SPOT6_201606301434572_FR1_FR1_SE1_SE1_W071S14_01871
Drone-derived Digital Surface Model (DSM)s and orthomosaics			
Qori Kalis Moraines II	17.09.2023	0.0165 m	785 images from DJI Mavic 2 drone Area covered: 0.2372 km^2 RMS Error (m) in XYZ: 0.45, 0.57, 3.87
Suyuparina forefield drone DEM	22.09.2023	0.032 m	552 images from DJI Mavic 2 drone. Area covered: 0.203 km^2 RMS Error (m) in XYZ: 0.41, 0.39, 0.81.
Quisoquipina Moraines drone DEM	22.09.2023	0.014 m	1971 images from DJI Mavic 2 drone Area covered: 0.201 km^2 RMS Error (m) in XYZ: 0.80, 1.18, 4.05

TABLE 2 *Mapping criteria for classification of landforms and surface features. After multiple sources (*Davies et al., 2022; Glasser et al., 2008; Lee et al., 2022; Leger et al., 2020; Małecki et al., 2018; Martin et al., 2019; McCerery et al., 2024*).*

Feature	Visual appearance on satellite imagery	Sedimentary characteristics	Significance
Topographic features			
Exposed bedrock (not ice-scoured)	Bedrock that is not noticeably ice scoured; structures remain visible. May be a scarp with a cliff, steep, sediment-free, strong colour variation due to geological control. Difference in colour to glacial sediments. Rough or lumpy appearance.	Sediment free bedrock	May form above trimlines and help quantify ice thickness. Often geologically controlled. Indicates limited till deposition and glacial abrasion.
Basalt and ignimbrite plateaux	Low-slope bedrock, dark colour (basalt) or light coloured (ignimbrite), flat plateau with steep scarp around	Exposed bedrock. Ignimbrite weathers to produce a coarse sand.	Uplifted areas that currently or previously held ice caps, such as Quelccaya Ice Cap
Mountain	Highest summit on the digital elevation model		Significant topographic feature
Glaciers			
Snowline	Transition from white snow to grey glacier ice. Higher albedo reflects a brighter white colour in snow. Snowlines mapped from Sentinel imagery listed in Table 1.		Indicates transition from zones of net accumulation to ablation. Features above this are largely snow-covered.
Crevasses	Dark grey lines on the glacier surface		Indicate ice-flow regime
Glaciers	White surfaces, smooth, occupying upper parts of the landsystem, may be crevasses and pockmarks visible.		
Supraglacial debris	Rough, brownish areas on the glacier surface, may be circular depressions, back-wasting scarps and boulders visible	Ice visible; thin and chaotic layer of gravel and boulders, typically angular	Indicates high debris input onto glacier ice.
Glacier cusps	Circular depressions on the glacier surface		Indicative of ablative processes
Subglacial landforms			
Overdeepenings	Parabolic-shaped valley, often with lakes or *bofedales* infilling the valley floor. Wide valley floor and steep-sided.	Large-scale features observed as over-widened, over-steepened valleys, often with specific over-deepenings infilled with lakes or *bofedales*.	Over-deepened, parabolic-shaped valleys are characteristic of erosive glaciated landscapes; contrasts significantly with landscapes dominated by fluvial processes and incision.
Drumlin	Depositional linear hills, oval to ellipsoidal shape, positive relief, aligned in the direction of former ice flow. Non-undulating and grey to brown in colour.		Associated with temperate ice flowing fast on low-gradient slopes, saturated sediments and deforming substrate.
Flutings	Linear, elongated, parallel features formed in sediment, often in groups, different to bedrock structure, ~1 m wide, 10–200 m long.	Ridges of sandy gravel and diamicton, often with a boulder or bedrock at their head, consistent orientation, contain faceted, edge-rounded and often striated clasts.	Indicative of former flow of warm-based ice, may be highly attenuated.
Rectilinear ridges (crevasse-fill ridges)	Short, straight and rectilinear lines, forming in cross-cutting lattice patterns. Discontinuous and small. May be too small to be visible on satellite imagery	Sharp-crested, small features, characteristic lattice framework	Marks injection of basal sediment into fractured glacial base followed by downwasting.
Streamlined bedrock lineation (roche moutonnée and whalebacks)	Highly linear, parallel ridges within areas of polished bedrock. Different colour to glacial sediments.	May show asymmetrical profile, a plucked face, abraded surface, striations, consistent orientation, associated with ice-scoured bedrock	Shows presence of plucking, abrasion and sliding; temperate ice; shows ice-flow direction. May suggest high ice-flow velocities.

TABLE 2 (Continued)

Feature	Visual appearance on satellite imagery	Sedimentary characteristics	Significance
Ice-scoured bedrock	Areas of bare bedrock, with visible inherent structures, dark brown to light grey, distinctive from sediment cover.	May show smoothing and striations as well as P-forms in the field	Shows areas of extensive ice at the pressure melting point.
Ice-marginal landforms			
Cirque	Bowl or amphitheatre-shaped depressions in the side of valleys or high relief ground		Indicates the headwall of glacier ice, characteristic of glaciated landscapes.
Trimline	Sub-horizontal lines on valley sides separating areas of glacial till and moraine and rough bedrock. Usually associated with latero-terminal moraines	Sharp altitudinal change, colour and texture difference	Indicates area of active erosion, especially the area glaciated during the Late Holocene neoglaciation, resulting in the freshest features.
Moraine	Moraine ridges are linear, curvilinear or arcuate. Ridges of positive relief, orientated parallel, subparallel or perpendicular to the valley side. Smooth texture distinct from bedrock.	Often found in association of glacially transported boulders. Sedimentary structure. Commonly subangular to subrounded clasts.	Mark position of former ice margin. Mapped showing the extent of the moraine.
Moraine crests	Crest along moraine.	Sharp crest, may have boulders	
Pedestal moraine	Moraines formed on top of large sediment accumulations composed of talus material, may be hundreds of metres high. Form from glacier flows onto thick debris accumulations raised above the valley floor (Iturrizaga, 2018).		Predominantly avalanche-nourished and debris-covered glaciers, though can be clean-ice. High sediment supply and poor removal capacity.
Hummocky moraine	Mounded appearance, dry and without wetland development, inside moraine crests.	Hummocky appearance with some order to the ridges. Strewn with boulders and kettle lakes. Subangular to subrounded clasts.	Marginal ice context. May indicate drying of the landscape following fluvial downcutting.
Kame terrace	Flat-topped surface above valley floor, extending from valley side, steep ice-contact face.	Visible in field as a large flat-topped feature, steep sided, extending down-valley, abruptly placed against steep valley side.	Marks position of former lateral or frontal ice margin, and indicates palaeoglacier ice thickness. Can indicate meltwater ponding at the lateral glacier margin.
Abandoned meltwater channel	These palaeochannels form shallow depressions or deeper incisions, may have gently or steeply sloping sides or scarps, incised into fluvial, glaciofluvial or glacial deposits. May be sinuous, braided and extensive. Currently contains no water.	Visible in the field as deep gorges or shallow laterally extensive channels.	Indicative for former river or stream flow.
Fluvial and lacustrine			
Lake	Smooth surface, dark blue to light grey colour. Found within overdeepenings and depressions.	Water is present	Ponding of water, often forming in over-deepened valleys.
Palaeosandar	Flat, well-drained area, may have meltwater channels developed on the surface.	Gravel, may have subtle meltwater channels, subangular to rounded clasts, some sorting of material	Indicates the former drainage regime of a glacier
Rivers and streams	Linear, sinuous water courses, may be surrounded by glaciofluvial sediments	Water present in the channel. May form a narrow braided gravel-bed river. May have silt-rich water from a high suspended sediment load.	Indicates the lowest elevation within a valley.
Gravel braided river	Valley-floor accumulations of sediment, light-grey colour, smooth surface, dissected by braided rivers and streams	Meltwater channels composed of gravel and boulders, outwash plains, subangular to subrounded clasts.	Glaciofluvial sediments, indicates a high sediment load

4 | GLACIAL GEOMORPHOLOGY OF THE CORDILLERA VILCANOTA

The mapped area (domain in Figure 1C; Figure 3; Supplementary Map) can be divided into three distinctive regions: (i) north of the Cordillera Vilcanota, with less extensive moraines; (ii) the Sibinacocha Plateau, with substantial and extensive moraines; and (iii) areas dominated by fluvial, rather than glacial, geomorphology, situated some distance away from the ice masses. Overall, within the domain, we mapped ~23,000 features, within six assemblages: topographic, glacier, subglacial, ice marginal, fluvial and lacustrine (Figure 3; Table 3).

Elevation transect AA (Figure 3, Figure 4) captures the difference in elevation north of the mountain range and onto the plateau, and the different distances from the ice divide of moraines deposited on either side of the ice divide. Elevation transect BB (Figure 4) shows the broad Sibinacocha Plateau, dissected by the wide river valley (Transect CC) and bounded by the steep mountains at either end.

Moraine sets follow names already used in the literature where available. For moraines with no names, we use the convention of naming moraines sequentially down-valley, named after the local river or valley. For example, in the Phinaya valley, the moraine set closest to the glacier are the 'Phinaya I' moraines, followed down-valley by the Phinaya II, III, IV, V and VI moraines.

4.1 | Glaciers

The study area contains several types of glaciers, including both shallow-gradient mountain glaciers such as Suyuparina and Quisoquipina glaciers, at the head of Quisoquipina valley (Figure 6; Figure 7); ice caps drained by outlet glaciers (Quelccaya Ice Cap and Qori Kalis Glacier, Figure 8); and steep mountain glaciers. There are also three small rock glaciers identified in the INAIGEM 2020 inventory (INAIGEM, 2023).

Suyuparina and Quisoquipina glaciers were visited during fieldwork in 2023 and 2024. The rapidly thinning (−0.92 m a^{-1}, 2010–2020 (Hugonnet et al., 2021)) Suyuparina Glacier, which in 2022 covered 0.75 km^2 and was just 1,493 m long, has an elevational range of 400 m and maximum ice thicknesses of 105 m (Millan et al., 2022). Like the adjacent Quisoquipina Glacier, the surface in the ablation zone is pockmarked with semicircular depressions, called here 'cusps' (Table 3; Figure 6B; Figure 7B). At the glacier termini are detached blocks or narrow 'sails' of glacier ice (Figure 7C), and the ice margin has a cuspate configuration that reflects the downwards ablation of the cusps. The terminus of Suyuparina Glacier forms an ice cliff ~20 m high with little evidence of deformation of ice (Figure 7A).

Vertical ice-marginal ice cliffs like this are characteristic of cold-based alpine-style glaciers and locations with high radiation and enhanced sublimation (Atkins, 2013; Lorrain & Fitzsimons, 2011). The low altitudinal range, thickness and low ice-surface slope (mean 10.7°) of Suyuparina Glacier also likely promote a limited gravitational driving stress and hence limit ice deformation. However, a small number of fragile bent icicles in subglacial cavities (Figure 7D) under the ice suggests the presence of at least some sliding as the ice moved slowly over the area. Sliding has been observed at other cold-based glacier margins (Atkins, 2013; Cuffey et al., 1999). The presence of flutes in the glacier forefield is also suggestive of sliding at the ice-bed interface (see: Subglacial assemblage) (Evans et al., 2010, 2012; Roberson et al., 2011).

4.2 | Subglacial features

Interpretations of the character of the subglacial environment come from two main lines of evidence: the large, wide, over-deepened glacial valleys and the landforms visible in the forefields of present-day glaciers, including flutes, polished, streamlined, ice-scoured bedrock and rectilinear ridges (Figure 5; Table 2; Table 3).

4.2.1 | Flutings

Flutes are common in proglacial areas (Figure 5; Figure 8; Table 3). These *en masse* flutes, which often have boulders or ice-scoured bedrock at their heads (Figure 7G), form an ensemble of streamlined and aligned sedimentary forms across large areas of the glacier forefields. They are commonly interrupted by small push moraines, and do not continue on the down-ice side of the moraine (Figure 6D; Figure 7H; Table 3).

Flutes have been observed in front of and beneath both temperate and polythermal glaciers (Roberson et al., 2011). The lodged boulders suggest that seeding was related to sediment deformation in a lee-side cavity under the ice (Evans et al., 2010). Squeezing sediment into cavities under the ice suggests that these landforms form under thicker, temperate ice, where meltwater is present and the substrate is deformable (Roberson et al., 2011). These flutings therefore indicate the presence of warm-based conditions within the recently deglaciated neoglacial moraine arc (Evans et al., 2012). This glacier forefield with well-developed subglacial bedforms such as flutings, combined with ice features suggesting a cold-based glacier terminus (see comments regarding Suyuparina Glacier above), indicates that Suyuparina Glacier, at least, is polythermal. However, other present-day thicker glaciers in the region may remain temperate throughout.

4.2.2 | Rectilinear crevasse-fill ridges

At Suyuparina Glacier numerous low-sinuosity, geometric, cross-cutting ridges were observed in the forefield (Figure 6; Figure 7F,H; Table 3). They overprint the flutes noted above. These ridges are interpreted to have formed as basal sediment was squeezed upwards within crevasses in glacial ice, thus preserving the spatial pattern of crevassing (Benn & Evans, 2010; Evans et al., 2012), and are commonly termed 'crevasse fill ridges', associated with ice stagnation (Evans et al., 2022; Rivers et al., 2023; Sharp, 1985). While delicate crevasse *squeeze* ridges are often associated with surging glaciers (Ben-Yehoshua et al., 2023), geometric rectilinear crevasse *fill* ridges could also form in environments such as the Suyuparina forefield where, in the cold, frozen ice marginal zone, rapid ablation in a high irradiation environment results in slow ice movement and rapid sublimation. Crevasse fill features such as these are associated with till squeezing in marginal environments into basal crevasses (Rivers et al., 2023). The overprinting of flutes indicates a switch in subglacial conditions at the glacier terminus, from a more warm-based

TABLE 3 Landform inventory from geomorphological mapping across the Cordillera Vilcanota. See Table 2 for landform identification criteria.

Feature	Number of observations	Total area, km^2	Mean area, km^2 (SD)*	Mean altitude, m asl (SD)*	Description
Topographic features					
Exposed bedrock (not ice-scoured)	273	62.52	0.2 (0.5)	5,085 (189)	Geological intrusions interrupt the landscape, with bedrock ridges prominent in the landscape. Ridges of bedrock or steep bedrock slopes, that have been subjected to little polishing or scouring under the glacier ice.
Basalt/ignimbrite plateau	2	36.9	18.4 (10.5)	5,141 (167)	Two main ignimbrite plateaux, in addition to the plateau beneath Quelccaya Ice Cap. Both plateaux are now ice-free and are located immediately south of Quelccaya Ice Cap, with surrounding moraines that suggest that ice caps existed here previously. Elsewhere, friable sedimentary rock form lower, softer and more rounded mountain ridgetops.
Mountain summit	13			5,814 (395)	4,958 to 6,384 m (Ausangate), with rugged exposed bedrock visible at high altitudes (Figure 3)
Glacier features					
Rock glaciers	3	0.09 km^2	0.03km^2	4,976 (12)	Mapped in the 2020 inventory (INAIGEM, 2023).
Snowline	25			5,280 (129)	A clear snowline is only rarely observed; many glaciers remain snow-covered to their tongues.
Crevasses	3,493			5,466 (174)	Transverse crevasses are widely observed on steep mountain glaciers, associated with extending flow. Rarely splaying crevasses observed at glacier terminus (e.g., Quisoquipina Glacier).
Glaciers (2022 inventory)	237	246.0	1.0 (1.6)	5,315 (169)	Glacier inventory from year 2022 AD.
Supraglacial debris cover	8	2.3	0.3 (0.6)		Most glaciers are clean ice, with only small areas of debris cover on the ice surface mapped (0.93%). All debris-covered glaciers were mapped around Mt. Pachanta (Figure 3). Only one glacier, which calves into a proglacial lake and drains westwards from Mt. Pachanta, has any significant proportion of its area debris-covered (37%).
Glacier cusps	281			5,345 (100)	Observed on the terminus of many glaciers, for example, Suyuparina and Quisoquipina glaciers (Figure 6B; Figure 7B), and terminus of Morajani Glacier on Quelccaya Ice Cap (Figure 8).
Subglacial features					
Drumlin	67			4,808 (145)	Large, regular, subdued, streamlined sedimentary ridges up to 10 m high, 800 m long and up to 180 m wide
Flutings	1,430			5,105 (161)	Common in relatively flat proglacial zones within the bounds of the Late Holocene moraines, where they extend down-ice aligned parallel to former ice-flow direction. Often with boulders at their heads. At Suyuparina Glacier (Figure 6; Figure 7), the sedimentary flutes extend linearly down-ice for distances up to 100 m, with fairly consistent heights (∼0.4 m) and widths (∼1.5 m). These flutes are composed of diamicton with large cobbles, and faceted and broken gravel clasts, which often exhibit clear striations. The flutes extend over both deformable substrate and diamicton. Flutes emerging from the ice at the ice margin show sediment deformation squeezed into elongated subglacial cavities (Figure 7E). These subglacial grooves at the ice margin show close association with deformed, bent icicles (Figure 7D).
Other streamlined landforms	10			4,845 (13)	Occur on the palaeosandar outside the Vilcanota Moraines I.
Boulder at head of flute	33				Where present, initiating boulders are typically subangular to subrounded with clear faceted faces, and often have a prow of sediment at their down-ice end.
Rectilinear crevasse-fill ridges	186			5,155 (15)	These sharp-crested rectilinear ridges are ∼1 m high and ∼0.2 m wide at the crest, and are formed of diamicton with edge-rounded, faceted and striated stones. They are symmetrical in cross-profile and orientated perpendicular or oblique to ice-flow direction. These rectilinear ridges with a small range of orientations are interpreted as crevasse-fill ridges.

(Continues)

TABLE 3 (Continued)

Feature	Number of observations	Total area, km^2	Mean area, km^2 (SD)*	Mean altitude, m asl (SD)*	Description
Streamlined bedrock lineation (roche moutonnée)	974			5,083 (244)	The roche moutonnées frequently have an abraded up-ice face with striae and a plucked face, as observed in the recently exposed forefield of Quelccaya Ice Cap.
Ice-scoured bedrock	466	62.9	0.1 (0.4)	5,049 (218)	
Ice-marginal features					
Trimline	107			5,055 (198)	Associated with, and often contiguous with, Late-Holocene moraines, denoting the margin of the last neoglaciation during the 'Little Ice Age'.
Moraine crests	11,479			4,921 (268)	Moraines were largely limited to an altitude of above 4,200 m and are sparse below this.
All moraine polygons	2,266	196.1	0.09 (0.3)	4,849 (292)	Range from large moraines with wide, rounded crests to fresh, sharp-crested moraines close to current glaciers
Angular boulders on moraine crest (from supraglacial rockfall)	248				Substantial supraglacial input from rockfall from surrounding topography, for example, at the Qori Kalis Moraines II (Figure 11)
Cirque	63				Widely observed in the mountain regions, often occupied by glaciers.
Abandoned meltwater channel	93				Occur between and through moraine crests, not currently occupied by meltwater
Kame terrace	1				Only example observed in association with the Quisoquipina Moraines II. Flat-topped terrace with elevation level with the col at the terminus of the moraines, interpreted to be the palaeo spillway for a moraine-dammed lake.
Fluvial and lacustrine features					
Rivers and streams	206				Form in the valley floors. Rivers fed by glaciers are often milky wide and form braided gravel-bed rivers.
Lake	1,079	62.5	0.06 (0.9)	4,828 (182)	Frequently form in the glacially eroded overdeepenings behind moraines, and on glacially scoured bedrock. Rare outside glaciated limits.
Palaeosandar	8	13.7	1.7 (1.5)	4,898 (68)	Forms outside moraines.

environment to a colder ice margin, likely as the glacier has thinned. The lack of abundant proglacial meltwater in this environment promotes preservation of these features.

Crevasse fill ridges were not observed at other ice margins visited (such as Qori Kalis Glacier), where often the larger altitudinal range and ice surface slope, deeper ice thickness and larger accumulation areas may promote a more substantial gravitational driving stress and more deformation of the ice at the ice margin.

4.2.3 | Ice-moulded bedrock

Polished bedrock characterised by striated, streamlined bedrock bedforms, such as roche moutonnées with plucked faces and whalebacks, are also common in the immediate forefield of many mountain glaciers, within the bounds of the inboard, inner moraines (Figure 5; Figure 8; Table 3). The polished bedrock recently exposed in front of Quelccaya Ice Cap also exhibits features such as scalloped, furrow-shaped, longitudinal P-forms (sensu Glasser & Bennett, 2004; Benn & Evans, 2010).

These regions of polished bedrock are especially common in front of the steeper mountain glaciers that are now receding up the steeper slopes of the mountains of Cordillera Vilcanota. Quarrying of bedrock to form the plucked faces of roche moutonnées has been associated with thin, temperate ice, where ice overburden pressure is low (Benn & Evans, 2010). Whalebacks may be more likely to form under higher ice overburden pressure where bed separation and cavity production are suppressed (Roberts & Long, 2005). Together, these features indicate that the ice-bed interface was temperate, with sliding, entrainment of debris within basal ice and abrasion and polishing of the bedrock through asperities entrained in the ice (Glasser et al., 2020). The P-forms indicate the presence of locally high basal meltwater pressures over the bedrock (Glasser & Bennett, 2004) and saturated till (Benn & Evans, 2010).

4.2.4 | Drumlins

Large, regular, subdued, streamlined sedimentary ridges up to 10 m high, 800 m long and up to 180 m wide are observed only in a couple of valleys (Figure 5; Table 3). The most convincing occurrence is in the valleys draining westwards from Quelccaya and flowing into the Qori Kalis Moraines II and the Quisoquipina Moraines II (Figure 5; Figure 8). These elongated ridges are long and occur in the valley

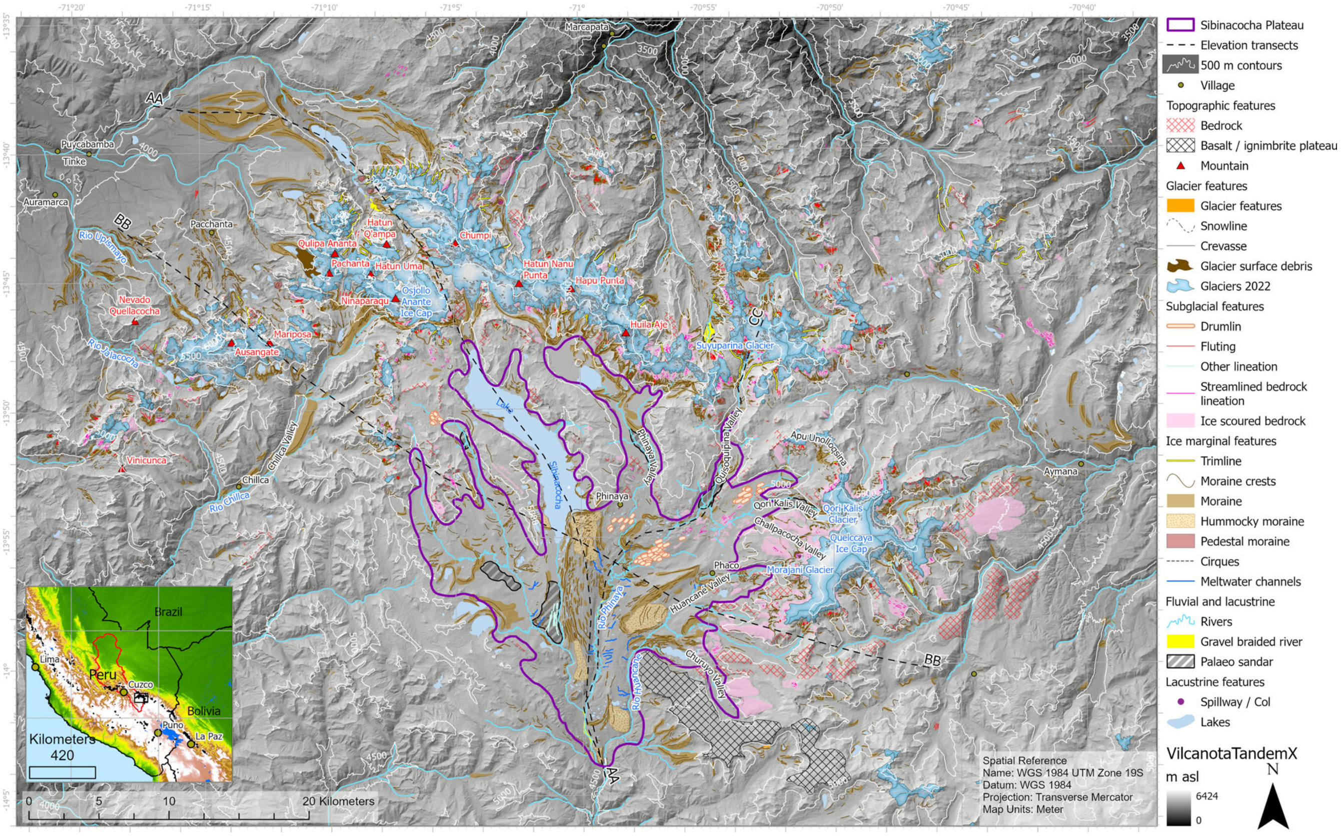

FIGURE 4 Overview geomorphological map of Cordillera Vilcanota and western Quelccaya Ice Cap, showing main landforms. The domain shows the area covered in this study. Elevation transects are shown in Figure 4. The inset shows glaciers (black), lakes (blue) and the Vilcanota-Urubamba catchment (red). Location of the main panel is shown in a black box. See Supplemental Online Map for further details. Landform inventory available in Table 3. Elevation data provided by TanDEM-X (12 m). Rock glaciers from the INAIGEM 2020 inventory (INAIGEM, 2023).

floor, separated by regions of streamlined bedrock. Though low relief, these features are characteristic of the length, width and size of drumlins (Ely et al., 2016, 2018; Spagnolo et al., 2010). Their arrangement in a regular field and alignment is also characteristic of drumlins (ibid.).

Drumlin forms like this are typically formed under thick, temperate ice masses, with coupled flow of ice and till (Clark et al., 2009; Ely et al., 2018, 2023; Stokes et al., 2013). While often associated with ice sheets, drumlins have also been observed under temperate glaciers (Jónsson et al., 2016). These features suggest that these glaciers had sufficient basal shear stress to deform subglacial sediment. They are, to our knowledge, the first examples of drumlins recorded in the tropics and altitudinally the highest drumlins recorded, though drumlins have been recognised at slightly lower altitudes in the Himalaya (Pall et al., 2019; Saha et al., 2016).

4.3 | Ice-marginal features

Regional geomorphological mapping around Cordillera Vilcanota and Quelccaya Ice Cap revealed previously unmapped moraines south of Lake Sibinacocha and across the Cordillera Vilcanota plateau (Figure 3; Figure 5; Figure 6; Table 3). These moraines indicate extensive southward-flowing lobes of ice on the Sibinacocha Plateau that coalesced from Cordillera Vilcanota and Quelccaya Ice Cap, with moraines forming ~50 km south of the ice divide. In the valleys between moraine sets, streamlined sedimentary and bedrock ridges record the passage of temperate ice flow and elucidate palaeoglacier ice-flow directions. Extensive moraines, first mapped by Mercer & Palacios (1977), are also visible north of the Cordillera Vilcanota massif, documenting northward-flowing lobes of ice. Cirques typically demarcate the upper limits of the glaciers of the northern sector of Cordillera Vilcanota. In the east, the plateau edge of Quelccaya Ice cap is also incised by cirques. Moraines were largely limited to an altitude of above 4,200 m asl and are sparse below this, reflecting the altitudinal (and resultant climatic) control that effectively limits the smaller ice advances north of the Cordillera Vilcanota ice mass.

Other ice marginal landforms include kame terraces, meltwater channels and trimlines (Figure 5). Kame terraces are very rare, suggesting limited glaciofluvial and glaciolacustrine activity. Abandoned meltwater channels commonly thread their way through and between moraines and are especially clear in the Late Holocene and more recently deglaciated regions. The poorly drained low points in the swales between moraines are now often a site for the development of *bofedales* wetlands. Trimlines clearly demarcate the extent of more recent glaciation, likely during the Late Holocene, often continuing from them towards the present-day ice limits (Figure 5; Table 3). These trimlines often bound ice-scoured bedrock with roche moutonnées.

In the sections below we describe the nested sequences of moraines in specific valleys: the Phinaya Valley, Quisoquipina Valley, Qori Kalis Valley and Huancané and Challpachocha valleys (see Figure 1, Figure 4 and Figure 6 for locations).

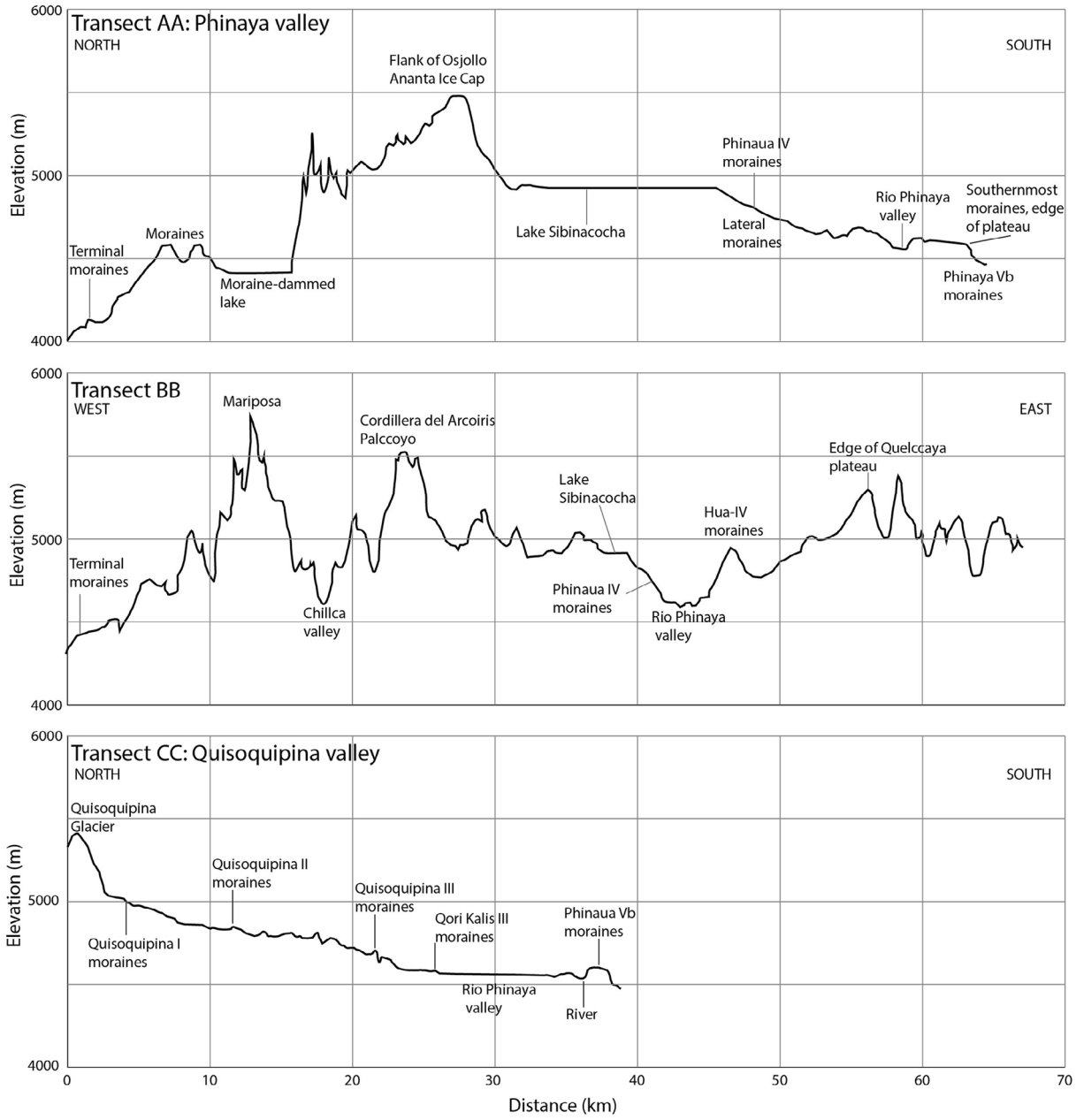

FIGURE 5 Elevation transects AA, BB and CC (see Figure 3 and Figure 5).

4.3.1 | Phinaya Valley

At the head of the Phinaya Valley, near the terminus of each glacier, at ca. 5000 m asl, there is an assemblage of flutes, small moraines and ice-scoured bedrock with roche moutonnées, bounded by large, fresh, unvegetated moraines, which link with clear trimlines in the lateral margins (Figure 6). These moraines typically have meltwater channels between and incised through the moraine crests and often enclose a lake within the over-deepened forefield. Clear trimlines typically demarcate the extent of the most recent neoglaciation and align with the latero-terminal moraines.

The innermost Phinaya I moraines near Lake Qasqara (Figure 6) are characteristic of these moraines. They are securely dated using cosmogenic nuclide ages to 0.2–0.7 ka (mean 0.2 ka, standard deviation 0.01), during the 'Little Ice Age' (Sagredo et al., 2016) (Figure 3B). The main moraine complex lies just 0.9 km from the present-day ice margin and, at 5035 m, over 100 m below the present-day ice margin. The well-defined main latero-terminal moraine complex is some 600 m wide and lies on the low-slope valley floor below the steep mountain glacier. In the swales between moraine crests, there are small boggy areas, with *bofedal* wetland development, and the moraine crests are cut by meltwater channels. The moraines are fresh-looking, sharp-crested and closely spaced and comprise a silty diamicton with numerous angular to subrounded boulders. The amplitude of each moraine crest is some 5 m and crest width is 1–2 m. Clast-form analysis at WP87 (Figure 11) shows some angular material likely derived from supraglacial sources given the overlooking topography, as well as more rounded and blocky clasts. Between this large moraine complex and the 2022 glacier terminus lie repeated small sawtooth-type moraines indicating the shape of the ice margin, with no evidence of crevasse squeeze ridges and few flutes.

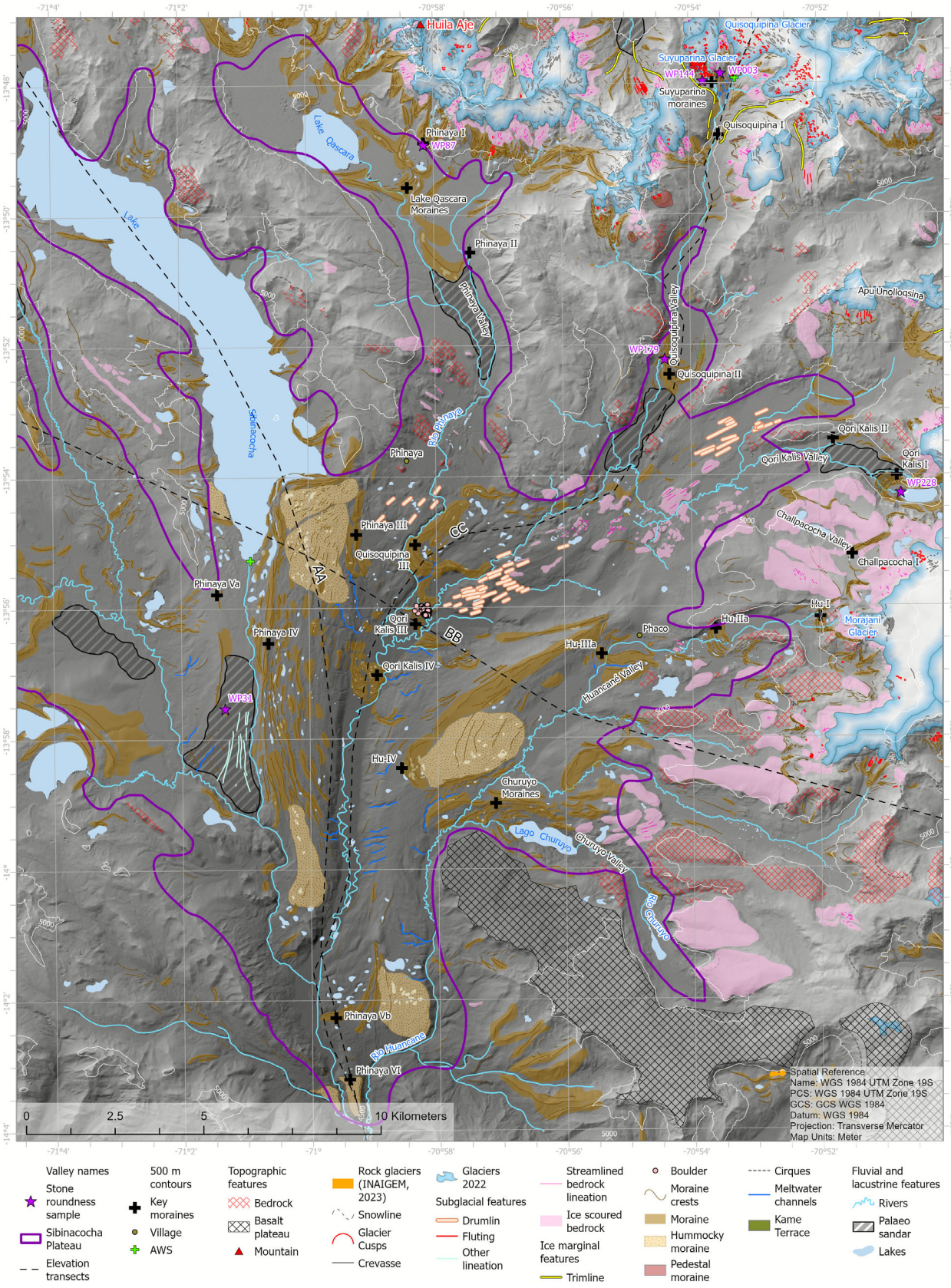

FIGURE 6 Geomorphology of the Sibinacocha Plateau, with moraine names mentioned in text. Transects shown in Figure 4. Shown on the hillshaded TanDEM-X. Rock glaciers from the INAIGEM 2020 inventory (INAIGEM, 2023).

Downstream of the Phinaya I moraines are the geomorphologically very similar and geographically adjacent Lake Qascara and Phinaya II moraines, indicating extended but separate glaciers in the upper parts of the Phinaya valley (Figure 6; Figure 10C). These moraines are located ~3.4 km down-valley from the present-day ice margin. They have rounded crests ~2 m wide, with proximal slopes of 12°. The moraines are approximately 20 m high. The Lake Qascara moraines encircle an overdeepening infilled with lake and *bofedal*.

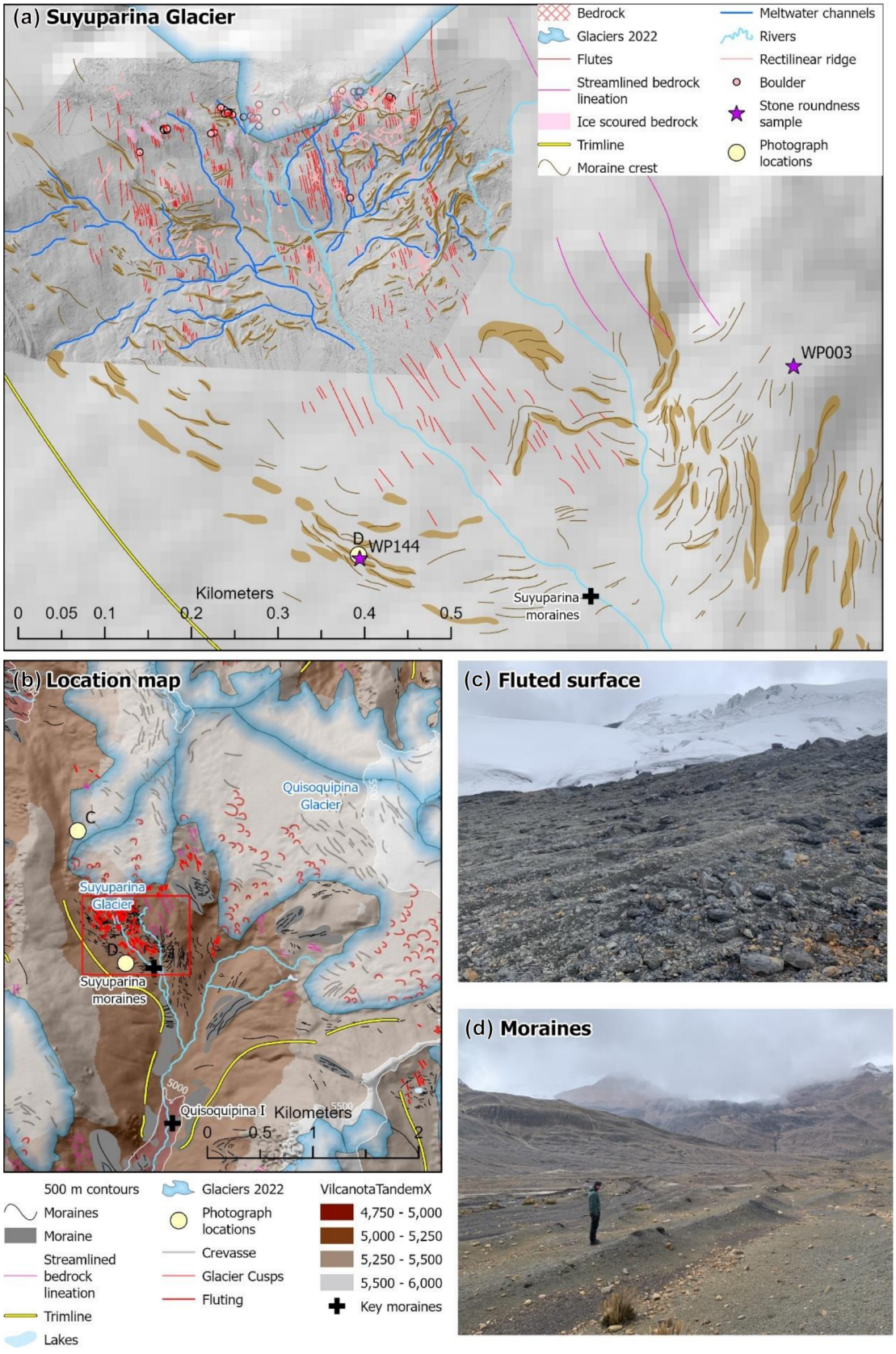

FIGURE 7 Suyuparina Glacier, at the head of Quisoquipina valley. A: Suyuparina Glacier forefield. Hillshaded drone-derived DEM is shown for the Suyaparina forefield (transparent polygon), superimposed on the Tandem-X hillshade. Flutings with initiating boulders where present, rectilinear ridges and moraines are shown. B: Overview of Suyuparina and Quisoquipina glaciers, with the location of panel A shown by red box. C: fluted surface at the present-day ice margin. D: small, sharp-crested moraines at the same location as pebble shape-roundness count WP144.

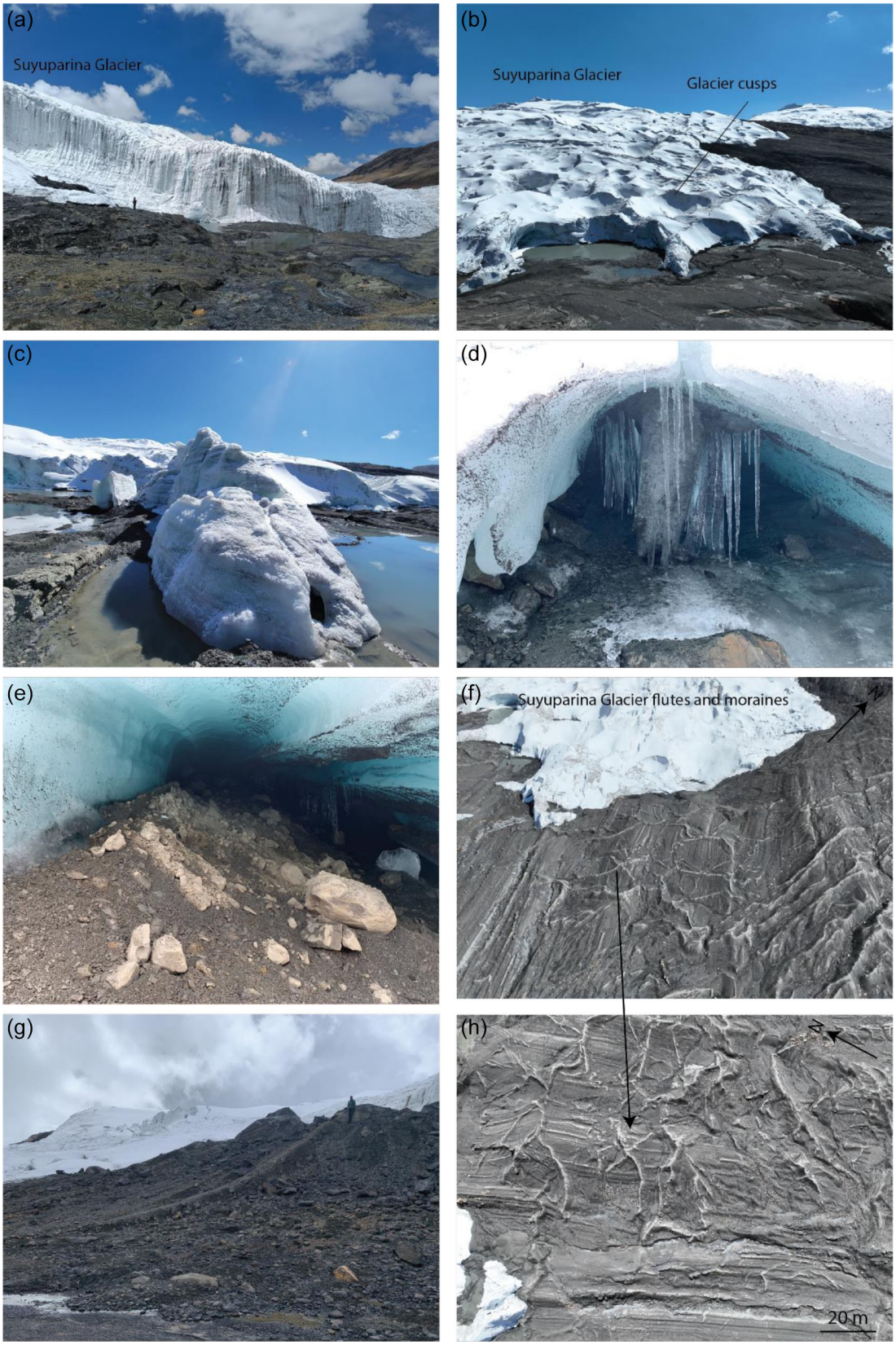

FIGURE 8 Photographs of Suyuparina Glacier terminus and forefield, at the head of Quisoquipina valley. A: Suyuparina Glacier, showing subvertical ice margin. B: Suyuparina Glacier and forefield. B shows the 'cusps' or potholes on the tongue. C: Sail of ice disconnected from the main terminus. D: A subglacial cavity. Surface melt has frozen overnight to form icicles, which are deformed as a result of glacier sliding. E: Subglacial grooved cavity, infilled with a flute. F: Drone image of the forefield of Suyuparina Glacier, showing moraines, flutings and geometric ridges interpreted as crevasse-fill ridges. G: Flute extending in the lee of a bedrock highpoint at the Suyuparina ice margin. H: Drone image showing detail of the glacier forefield.

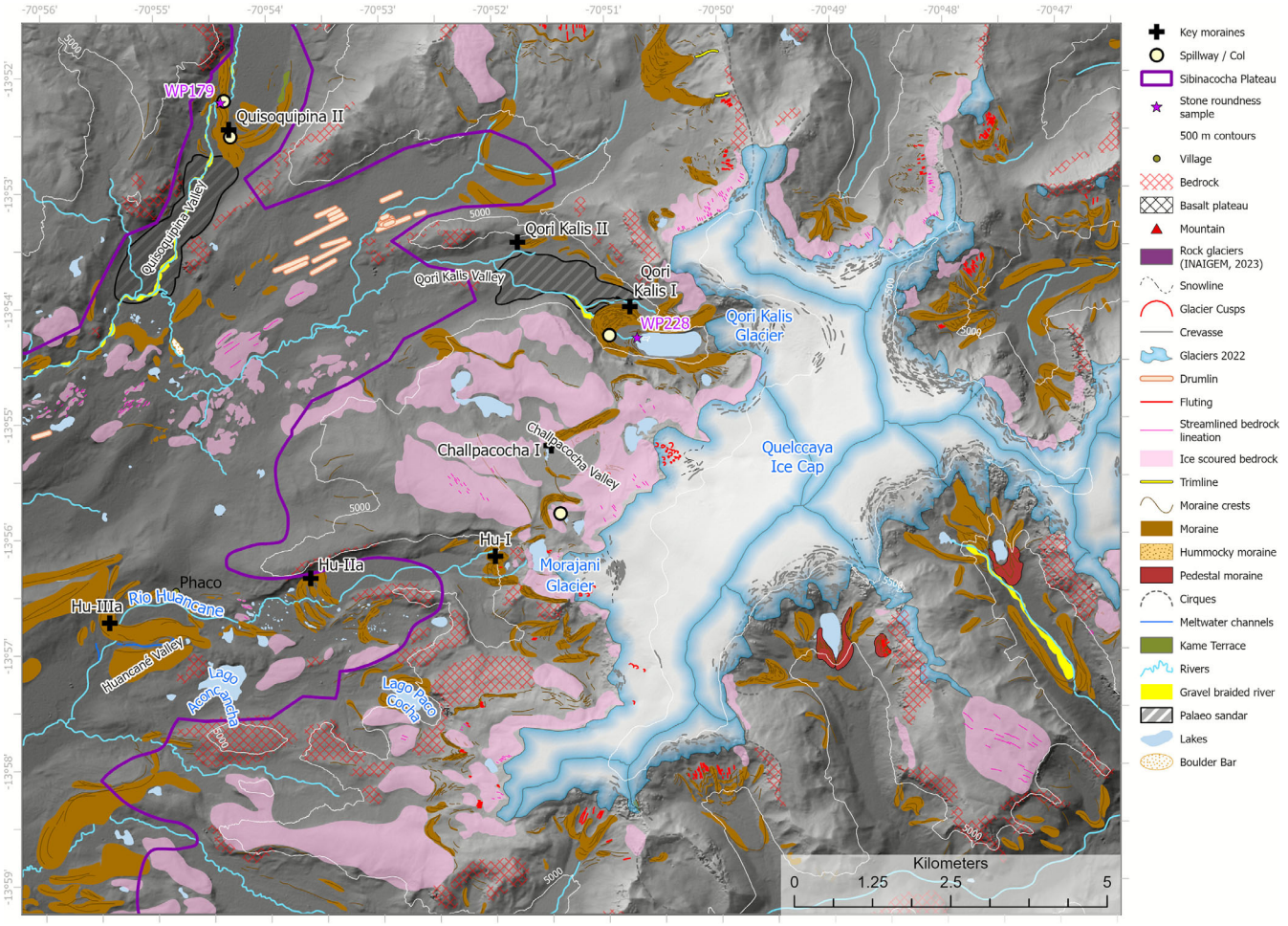

FIGURE 9 Quelccaya Ice Cap glaciology and geomorphology.

Boulders litter the ridge crest, ranging from angular to faceted with edge-rounded corners. The series of moraines continues down-valley. South of the village of Phinaya are the Phinaya III moraines, which may represent a final glacier stabilisation before the ice lobes separated into their different valleys.

South of Lake Sibinacocha, down-valley and stratigraphically older than the up-valley moraines, are the comparatively more voluminous Phinaya IV moraines, forming along the western edge of the Río Phinaya valley (Figure 6D,E). This lateral-terminal moraine complex comprises multiple moraine crests, with hummocky moraine extending down the valley side towards Río Phinaya (Figure 10E). The largest outer moraines have clear, rounded ridge crests up to 10 m wide, containing a hummocky topography with common kettle lakes and common boulders with a b-axis of >1 m of a wide range of lithologies. River cuttings here reveal clast-rich, matrix-supported diamicton covered with river gravels (Figure 10D). These moraines reflect a substantial advance of the ice lobes, extending some 50 km down-valley from the present-day ice margin.

Outside of these moraines are the Phinaya V moraines. The Phinaya Va moraines are lateral moraines from the Phinaya ice lobe, located west of the Phinaya IV moraines (Figure 6, Figure 10F). The Phinaya Va moraines comprise a north–south trending ridge crest, littered with boulders of varying lithologies, commonly faceted. The ridge is broad and 10–15 m wide, and up to 30 m high, extends from the southern margin of Lake Sibinacocha, and is exactly parallel with the Phinaya VI moraines. The moraine comprises a pebble and cobble-rich diamicton. Pebbles within the diamicton (WP31; Figure 11) are mainly subrounded to subangular, and blocks to slabs in shape, typical of subglacially transported clasts (Benn & Ballantyne, 1993; Lukas et al., 2013).

The moraine stratigraphy shows that at the time of moraine formation, the ice lobes had separated from ice flowing from the east into distinctive lobes, one occupying the Phinaya river valley and one flowing from ice sourced from Cerro Comercocha. The flat ground between the Phinaya Va and Phinaya IV moraines may indicate that a sandur previously occupied this area.

The Phinaya Vb moraines are arcuate terminal moraines, located down-valley of the Phinaya IV terminal moraine complex. The Phinaya Vb and slightly more ice-distal and final Phinaya VI moraines are both characterised by a hummocky, degraded appearance, wide and low ridge crests and scattered boulders. The ridge crests are wider and more hummocky than the up-valley Phinaya IV moraines. The hummocky moraine surface within the moraines is bounded by substantial fluvial incision and river terracing.

Finally, the Phinaya VI moraines (Figure 10G) reflect the southernmost limit of the ice lobe that occupied the Phinaya valley. They are stratigraphically the oldest and most ice-distal in the study domain.

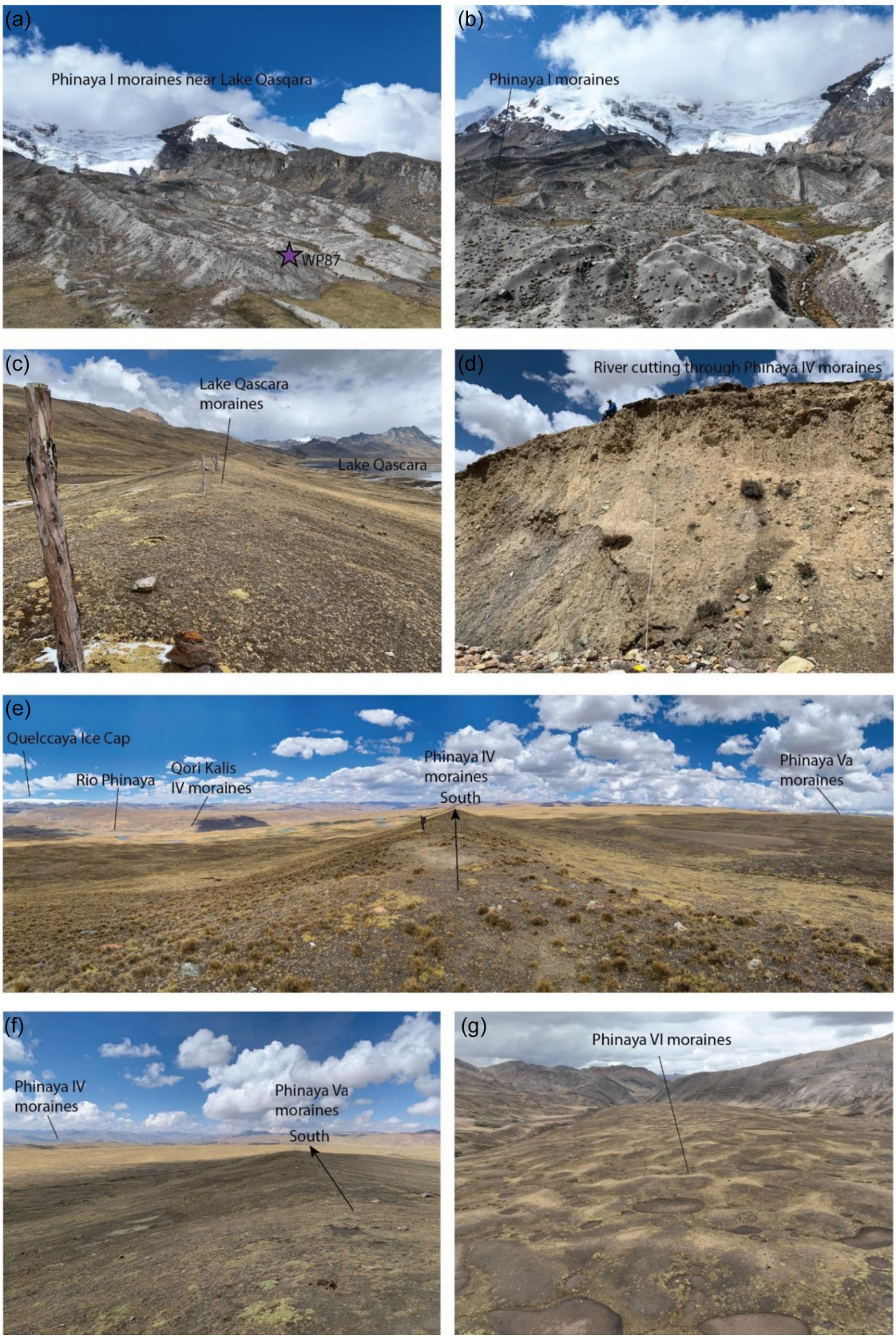

FIGURE 10 Examples of moraines from the Río Phinaya valley.

4.3.2 | Quisoquipina Valley

Access to the Suyuparina Glacier terminus at the head of Quisoquipina Valley allowed observation and analysis of moraines in the immediate ice environment, using field and drone surveys. The forefield of Suyuparina Glacier covered by the drone-derived DEM in Figure 6A lies within the boundary of the RGI glacier outlines dated to the year 2003 (RGI 7.0 Consortium, 2023). This area, which has an even, mean slope of 18°, is characterised by multiple small moraine ridges up to 1–3 m high, with symmetrical proximal and

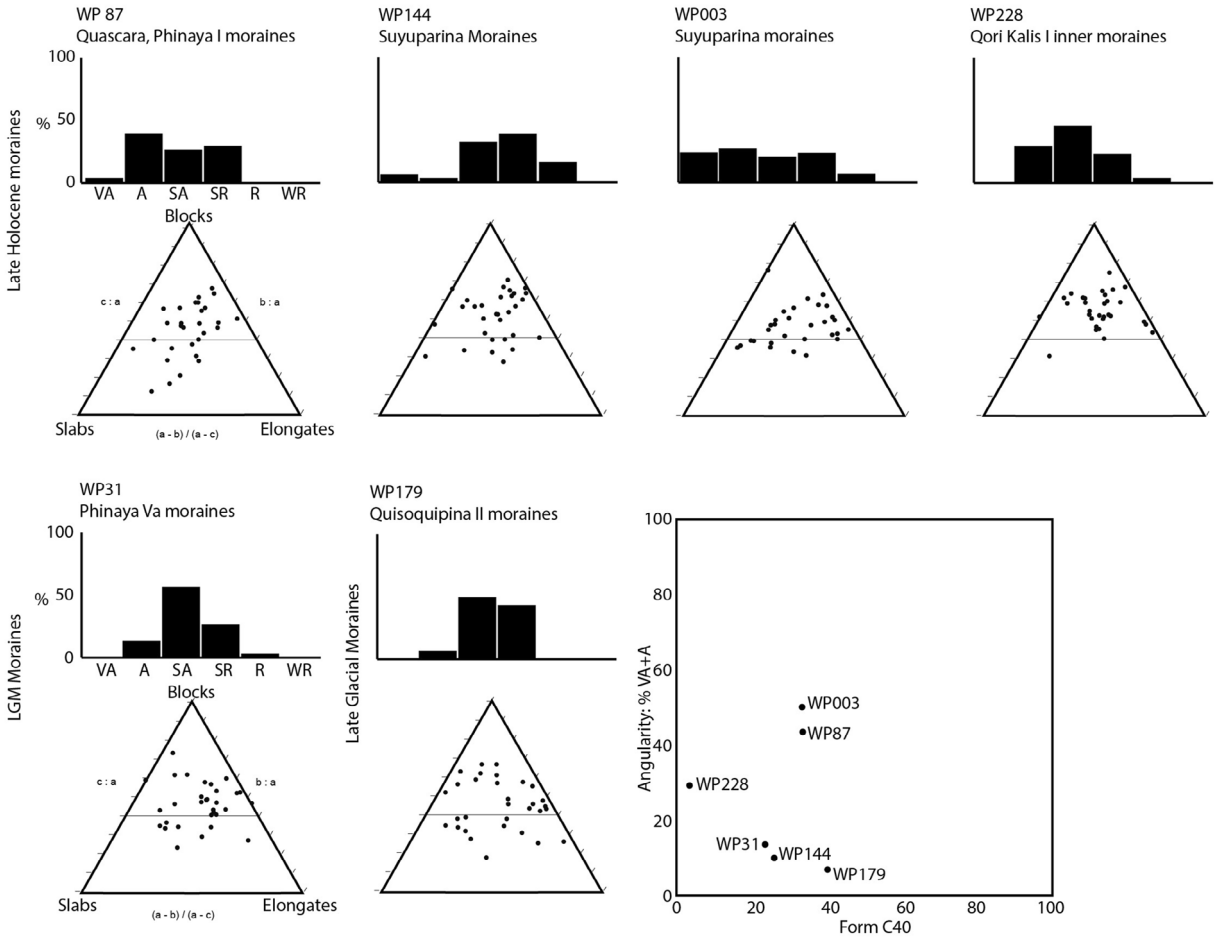

FIGURE 11 Clast-form analysis from moraines around the Cordillera Vilcanota plateau. Locations in Figures 6, 7 and 9.

distal slopes of ~20–50° and comprised of a shale-rich silty diamicton. These Suyuparina Moraines (Figure 7; Figure 12A) comprise ridges that are sharp-crested, and unlike the prominent mid-valley moraines lower down-valley, form a sequence of repeated moraine crests 5–20 m apart (Figure 6D; Figure 7F,H). These moraines cross-cut abundant flutes and crevasse-squeeze ridges that are abundant within their limits. The moraines are arranged in an arcuate shape across the foreland (Figure 6A) and meltwater channels from the ice margin flow in between the moraine crests, eventually forming a braided stream.

A clast form analysis count from a latero-terminal moraine in the Suyuparina Glacier forefield (WP 144; Figure 6A,D; Figure 7) yielded numerous faceted and striated clasts, with a dominance of subrounded and subangular pebbles and cobbles (Figure 11). No evidence of degrading ice cores was observed in the moraines. The clast edge rounding and the striations and faceting are indicative of active glacial transport and imprinting within the subglacial traction zone and indicate temperate ice conditions (cf. Małecki et al., 2018).

The RGI outlines indicate that the moraines exposed here are less than 20 years old, and, given there is a sequence of approximately 20 moraine crests within this area, they are likely formed annually. These small moraines are typical of push moraines formed at an ice margin with at least partially an active-temperate thermal regime (Bradwell, 2004; Chandler et al., 2020).

A total of 1750 m down-valley in the Quisoquipina valley are the Quisoquipina I moraines (Figure 6; Figure 12B), which are morphostratigraphically similar to the Phinaya I moraines dated securely to the 'Little Ice Age' (Sagredo et al., 2016) (Figure 3B). These moraines link to trimlines indicating an enlarged and coalescent Suyuparina and Quisoquipina Glacier occupying the head of Quisoquipina valley at this time.

Where there is high rockfall input, moraines crop out as pedestal moraines, raised above the valley floor on a 'pedestal' of talus, forming the perched 'pedestal moraines' as seen in other regions of Peru (cf. Iturrizaga, 2018). There are only a few examples in the Quisoquipina valley, on the valley sides, and in other locations, such as at Montaña de Siete Colores (colloquially 'Rainbow Mountain' or *Vinicunca*) or Cerro Comercocha (see Figure 4 for locations). This is because, compared with other regions of Peru, large rock walls supplying abundant supraglacial debris are relatively rare.

A 9 km down-valley from the glacier terminus are the Quisoquipina II moraines (Figure 6; Figure 12C). These arcuate moraines extend across the Quisoquipina valley and comprise a multi-crested latero-terminal moraine complex. The moraine matrix material exposed in the river cutting at WP179 shows the moraine to comprise a massive matrix-supported, gravel-rich diamicton with abundant cobbles and boulders. Stones are commonly faceted and edge-rounded and include a range of lithologies, including porphyries, granite, sandstone, shales and rhyolites. A clast-form analysis count at WP179 (Figure 11) shows a dominance of subrounded to subangular clasts. Abandoned palaeochannels at the apex of the moraine and flat-topped terraces interpreted as kame terraces within the Quisoquipina

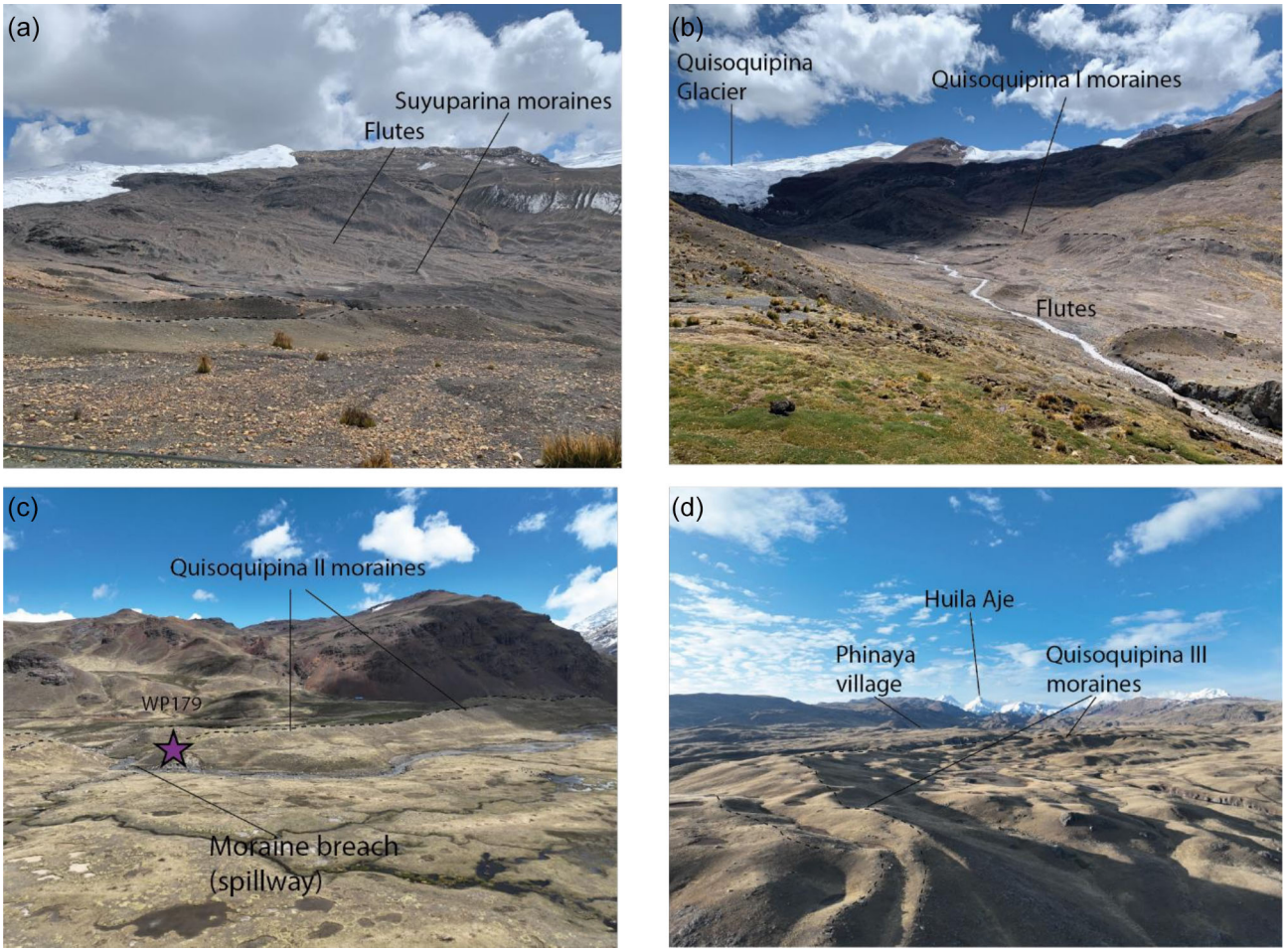

FIGURE 12 Moraines of the Quisoquipina Valley. For locations see Figure 6. Dashed black lines pick out moraine crests.

II Moraines, and sorted clays present within exploratory shallow Russian Core samples, indicate the presence of a former moraine-dammed lake, which eventually drained through the fresher moraine breach located at WP179.

These moraines are typical of temperate valley glacier terminal moraines and reflect both a substantial, easily erodible debris supply and temperate glaciers able to erode, transport and deposit material within the subglacial traction zone (Evans & Twigg, 2002). These large moraines reflect quasi-stable positions of the ice margin, with glaciers temporarily in equilibrium with the environment (Evans, 2013). The Quisoquipina II moraines reflect a glacier that was stable within the valley, independent of ice from Quelccaya or the Phinaya valley.

Downstream of these, some 16 km from the current ice margin, are the substantial Quisoquipina III moraines (Figure 6; Figure 12D). This moraine complex is contiguous with the Qori Kalis III moraines, but indicates an ice margin independent from the ice lobe in the Phinaya valley. Moraines are broad, multi-crested, with numerous scattered boulders.

4.3.3 | Qori Kalis Valley

At the head of the Qori Kalis valley, fresh moraines enclose a proglacial lake (Figure 6; Figure 13). The Qori Kalis I moraines comprise a piedmont lobe spreading out from the valley confines onto the wide, flat valley floor. The main moraine complex is some 600 m wide and comprises multiple moraine crests with meltwater channels between (Figure 13). The moraines are sandy, reflecting the ignimbrite sources available up-glacier and contain numerous ignimbrite boulders, some of which are striated and which are commonly edge-rounded and faceted. The innermost moraines at the lake margin contain numerous angular boulders, suggesting significant supraglacial input at this point; this is reflected in the clast angularity at WP228. Ice-polished bedrock is visible at the ice margin above the lake. ^{10}Be exposure ages from boulders on the Qori Kalis I moraines securely date these most recent moraines to the latest Holocene, ca. 0.2 to 0.5 ka (Stroup et al., 2014) (Figure 3).

The Qori Kalis III moraines, some 14.8 km down-valley from Qori Kalis Glacier, are much broader than the valley glacier moraines up-valley and are similar in characteristics to the Quisoquipina III moraines (Figure 6; Figure 13). They have well-rounded ridge crests, with meltwater channels and rounded kettle lakes on and between crests. The moraine crest is almost flat, with sparse scattered boulders.

Where there is overlooking topography, supraglacial debris input is evident in some of these mid-valley moraines. For example, one small part of the Qori Kalis III moraines contains abundant blocky and angular monolithic boulders, reflecting substantial rockfall input from just up-valley (Figure 14; Table 3), as well as a sandy texture reflecting the breakdown of ignimbrite boulders sourced from further up-valley.

The most ice-distal moraines from ice in the Quisoquipina Valley, indicating ice independent from the Phinaya ice lobe, are

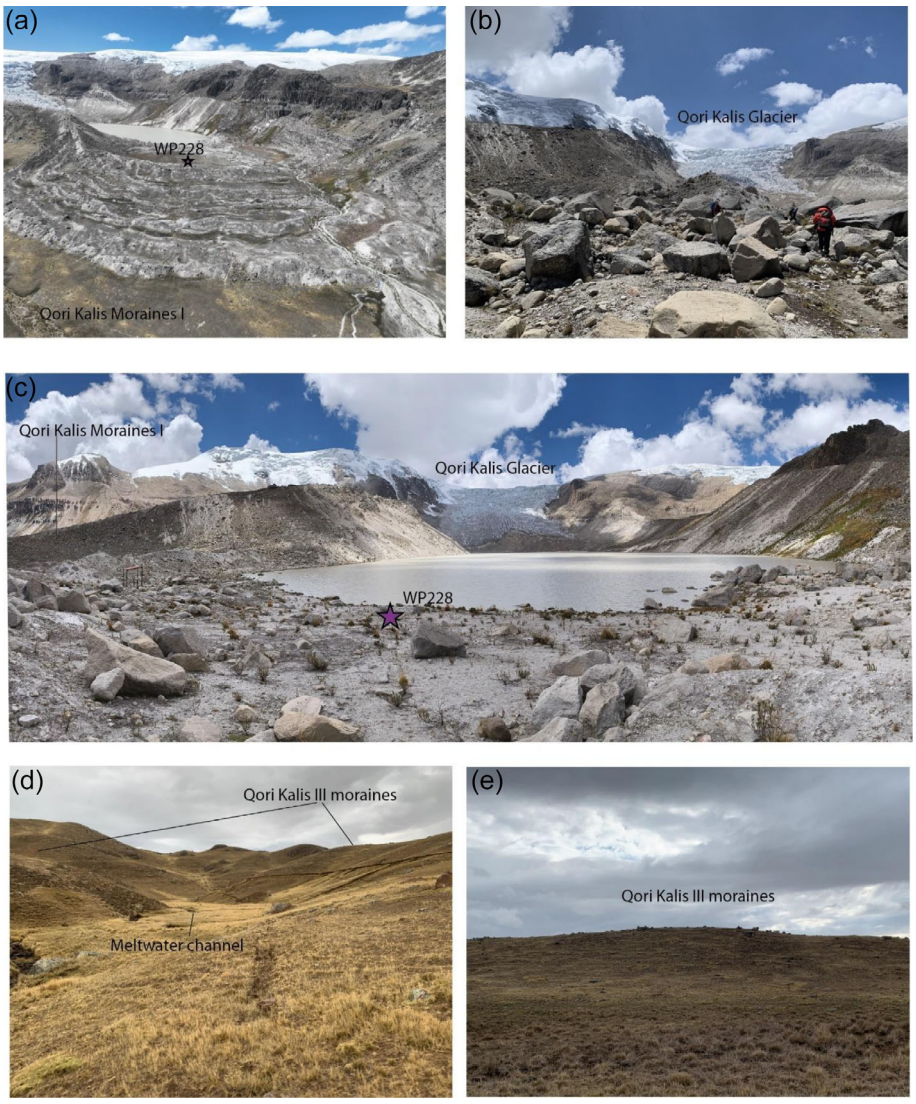

FIGURE 13 Qori Kalis Glacier and Qori Kalis I moraines.

the Qori Kalis IV moraines. These moraines are located on the Phinaya River valley floor and are strongly washed and incised by the Río Phinaya.

4.3.4 | Huancané and Challopachocha valleys

The Huancané and Challpachocha valleys contain most of the chronological data in the study area (Figure 3C). The Hurancané valley contains a similar suite of nested moraines to that of the Quisoquipina valley, with the Hu-I moraines near Marajani Glacier likely representing a readvance during the Little Ice Age, coeval with the Qori Kalis I and Phinaya I moraines (Figure 9). The large Challpacocha I moraines of western Quelccaya (Figure 3C) yield slightly older ages of 0.8–1.8 ka, suggesting another late Holocene advance (Stroup et al., 2015). At 3.8 km from the ice margin down the Huancané valley, the Hu-IIa moraines in the Huancané Valley yield tightly clustered boulder cosmogenic nuclide exposure ages of 11.3 to 11.9 ka (Kelly et al., 2015) (Figure 3C).

At 1,600 m further down-valley, the Hu-IIIb moraines (Figure 9) have cosmogenic nuclide exposure ages of 13.0 to 14.0 ka (Kelly et al., 2015) (Figure 3C). The Hu-IIIa moraines, another 1,300 m down-valley and a total of 7.3 km from the year 2022 Morajani Glacier margin, are dated to before ~14.2 cal. ka BP by radiocarbon ages in a kettle lake inside the moraine arc (Mercer & Palacios, 1977) (Figure 3C). These well-dated Hu-III moraines are ascribed to the Antarctic Cold Reversal. Finally, the Hu-IV moraines occupy the valley-mouth position, 13 km down-valley from the contemporary ice margin, and are geomorphologically similar to the large Qori Kalis III and Quisquipina III moraines. In the adjacent Río Churuyo valley to the south, the Churuyo moraines also occupy the valley mouth position (Figure 6).

4.4 | Fluvial and lacustrine features

Most valleys are occupied by rivers at their floor, which often flow into wetlands. These rivers occur as milky-coloured gravel braided rivers, reflecting their high suspended load. These small-scale glaciofluvial braided rivers are indicative of the low-meltwater environment, with limited precipitation in the dry season (Figure 2). At higher altitudes, ablation is dominated by sublimation; at the summit

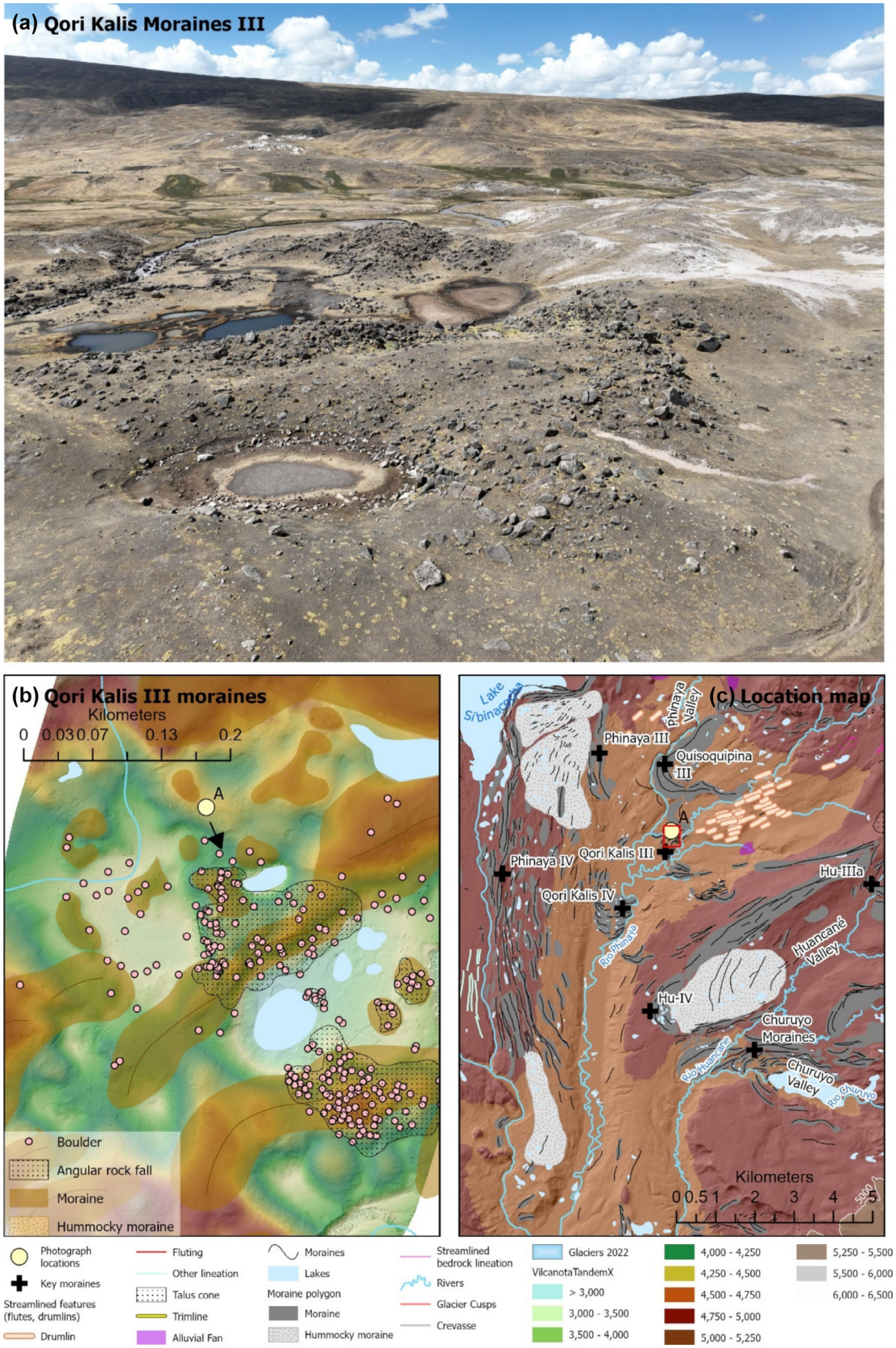

FIGURE 14 Qori Kalis III moraines with angular rockfall. A: Drone image of the moraines, showing angular blocky rockfall on the moraine surface and small kettle lakes. B: Hillshaded drone-derived DEM of the Qori Kalis Moraines II with regions of rockfall mapped. Location of camera in panel A, and direction of the photograph is shown. C: location map; red box shows location of panel B.

of Quelccaya Ice Cap, sublimation accounts for 81% of ablation (Fyffe et al., 2021). However, larger palaeosandar mapped beyond the moraine suggests a more active glacier-hydrological system during larger palaeoglacier extents.

Many of the glacially eroded overdeepenings behind moraines are occupied by moraine-dammed lakes, and bedrock-dammed lakes are common in the areas of exposed bedrock. Small lakes also occur frequently in kettle lakes between and behind moraines, often

associated with abandoned meltwater channels. Lakes are sparse outside the glaciated region. These fluvial and lacustrine landforms are covered in more detail in Davies et al. (submitted).

5 | DISCUSSION

5.1 | Glacier dynamics

At Suyuparina Glacier, evidence of deformable ice and substrate under temperate conditions includes the flutings, annual moraine formation and the formation of glacial till alongside striated and polished bedrock and cobbles. Conversely, evidence of a frozen margin includes the preservation of delicate crevasse squeeze ridges (Evans et al., 2022; Rivers et al., 2023; Sharp, 1985) and the vertical ice cliffs with little evidence of ice deformation. This assemblage together suggests a polythermal zone at the ice margin, with flutes formed further up-glacier under thicker ice and preserved under a cold glacier snout with limited ice deformation (Evans et al., 2012; Roberson et al., 2011). This is likely to occur under many of the smaller glaciers in the region.

Conversely, the larger, steeper mountain glaciers and the glaciers draining from Quelccaya Ice Cap have an assemblage dominated by large and repeated nested neoglacial moraines, with abundant scratched and polished cobbles, striated and polished bedrock and overdeepenings infilled with *bofedales* wetlands or lakes and lack the polythermal ice margin assemblage. Their greater size, thicker ice (cf. Millan et al., 2022) and larger accumulation area likely results in temperate ice throughout. This is aided by the fact that there is a limited seasonal variation in air temperature, with seasonal means at 5000 m asl remaining just above 0°C year-round (Schauwecker et al., 2017).

The larger moraines (e.g., Phinaya VI, Phinaya Va, Quisoquipina II and III moraines, Qori Kalis III), likely dating from the Holocene, Late Glacial and Last Glacial Maximum periods, are typical of temperate glacier environments, with evidence of polishing bedrock region-wide, the formation of drumlins along ice-flow corridors and the erosion and deposition of substantial moraines and features. The large size of the moraines likely reflects the volume of readily available sediment within the catchment from friable bedrock. This also reflects the processes of sliding, lodgement and ice deformation within the temperate glaciers, evidenced by striated, faceted and edge-rounded boulders and cobbles.

5.2 | Palaeo-icefield reconstruction

We used these geomorphological and chronological datasets to reconstruct a palaeo-icefield, with multiple topographically constrained ice lobes flowing across the plateau (Figure 15). We use the outer moraine limits in each valley to demarcate the maximum icefield

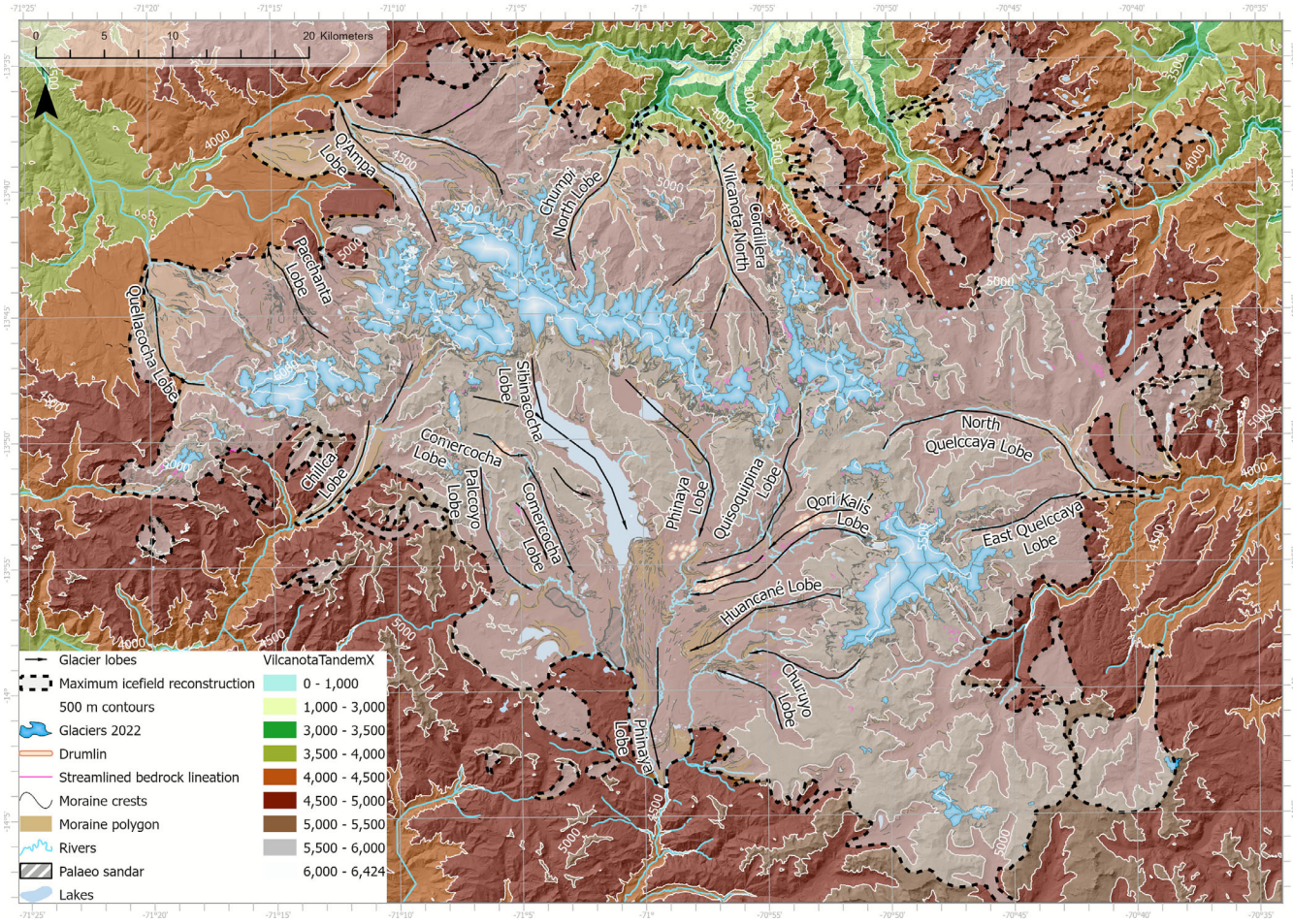

FIGURE 15 Cordillera Vilcanota Icefield reconstruction for the maximum glaciation extent, with ice flow directions constrained by geomorphology.

reconstruction. Ice flow lobes are reconstructed using indicators of ice flow (e.g. streamlined bedrock, drumlins, flutes), topography and elevation and the pattern of moraines in each valley, following previous practice (e.g. Davies et al., 2020). We note that the icefield reconstruction has limited data to constrain ice thickness or vertical development, though interactions with topography are well constrained by geomorphology.

The substantial Cordillera Vilcanota North and the Chumpi North lobes flowed northwards. At the southern limit of the plateau, these lobes coalesced to form the large South Vilcanota Lobe, which crossed to the lower limit of the Sibinacocha Plateau. Overall, the main icefield was >70 km across in the east–west direction and ~50 km across in the north–south direction. The main icefield covered 2,413 km^2 with a total area of 2,700 km^2 across the domain (Figure 15).

The icefield was surrounded by numerous mountain glaciers and smaller icefields, with lobes of ice extending down from the main mountain range. The glacier termini likely reached their lowest elevations on the northern side of the ice divide. Here, the Cordillera Vilcanota North lobe has moraines at an elevation of 3,500 m asl, with the lobe forming a glacier 21.5 km long from the contemporary ice divide to the terminus. The nearby Chumpi North Lobe reaches 3,160 m asl, perhaps reflecting the large accumulation area and height of the Chumpi Massif. Further expansion was likely limited by the rapid loss of altitude northwards (Figure 13). The Chumpi North Lobe reaches 16 km from the contemporary ice divide to the lowest terminus. In the west, the Q'Ampa Lobe and the Quellacocha Lobe reach 4,120 m asl and 4,000 m asl, respectively.

The southerly flowing lobes do not reach such low altitudes; the lowest terminus of the Chillca Lobe lies at 4400 m asl, and the Phinaya Lobe remains just above the 4,500 m contour. These glaciers are, however, longer, with the Phinaya Lobe reaching ~35 km from the ice divide to the terminus. As the palaeoglaciers receded, they separated into the Huancané and Qori Kalis lobes, draining from Quelccaya Ice Cap; Quisoquipina lobe, draining from Suyuparina Glacier and Quisoquipina Glacier; and the upper Phinaya Lobe and Sibinacocha lobes, both draining from the main massif (Figure 14). Glaciers draining eastwards from Quelccaya include the North and East Quelccaya lobes, which converge and terminate at ~4,300 m asl. These differences in altitude and size likely reflect not only the topographic constraints on the icefield, but also the dominant wind-borne moisture sources at the time of maximum glaciation, likely associated with airstreams arriving from the Amazon, as is the case today.

5.3 | Morphostratigraphic reconstruction

Our geomorphological mapping identifies multiple nested moraine sequences across the study area. We focus here on the Sibinacocha Plateau, where the moraine record is most complete, and where field surveys were focused, providing the most comprehensive observations. There is a clear morphostratigraphic and geomorphological variation down-valley, with clear ridge-crest lowering and widening. A repeated pattern is visible across the different valleys. These differences indicate the differential passage of time between the formation of moraine sets, with stratigraphically older, more ice-distal moraines being subjected to more subaerial weathering processes. We used morphostratigraphic differences, stratigraphic position, patterns of moraines, indicators of ice flow (drumlins, flutes, streamlined bedrock, topography), published chronological data and the ice-lobe reconstructions to identify seven clear ice margins, hypothesised to be stratigraphically correlative across the study region (Figure 16).

Here, we present an initial morpho-stratigraphic correlation of moraines across the study area and suggest a preliminary temporal framework, anchored by published ages where available. The large and most ice-distal outer moraines are the stratigraphically oldest moraines in the area. Of these, the oldest Phase 1 Phinaya VI moraines represent the southern limit of the Phinaya Lobe at the margin of the plateau, and the most extensive ice margin. We tentatively ascribe this advance to during or prior to the gLGM. Radiocarbon dating from the outermost moraines north of the icefield, around Pacchanta (Figure 3A, up to 35.6 cal. ka BP; (Mercer & Palacios, 1977)), supports a large advance that predated the gLGM, as do studies from other regions of Peru (Smith et al., 2005a).

Phase 2 is defined by a distinctive terminal moraine ridge (Phinaya Vb moraines) and represents temporary stabilisation during retreat. By Phase 2, the glacier outlet lobes are topographically confined and, in the west, the Comercocha Lobe and the Phinaya Lobe are separated, as indicated by the presence of the Phinaya Va lateral moraines. The Phase 2 moraines (Phinaya Va and Vb) have a lower elevation north of the ice divide than south, and are generally the lowest in elevation of those across the study area (Figure 16). For example, the stratigraphically oldest moraines in Chumpi North Lobe, ascribed to Phase 2, have a ZMean of 3,604 m, compared with 4,658 m asl for Phinaya Lobe. The stratigraphically oldest and most ice-distal moraines of the Q'Ampa Lobe, in the northwest of the study region, have a ZMean of 4,467 m asl.

The morphostratigraphically younger Phase 3, with fresher, less weathered moraines, mainly includes the latero-terminal Phinaya IV moraines south of Lake Sibinacocha. Phase 3 moraines are also tentatively indicated in the middle of the valley for the Palccoyo Lobe. The Phase 3 moraines have less hummocky topography and clearer moraine crests. The ice lobes are clearly topographically confined, with the Phinaya Lobe occupying the Phinaya valley, sustained by ice from Quelccaya and Quisoquipina, separated from the ice from the east (Palccoyo Lobe, Comercocha Lobe) (Figure 16). A sandar may have formed in the ice-free land between these ice lobes at this time.

The ice marginal position of the Phinaya Lobe during the global Last Glacial Maximum (late MIS 2) likely lies between the Phase 1 and 3 moraines, though this awaits further testing with numerical ages. Here we tentatively ascribe Phase 1 and 2 to prior to the global LGM and Phase 3 to late MIS 2 (cf. Hall et al., 2009; Smith et al., 2005b; Zech et al., 2009). This advance of 50 km at the maximum ice margin position is far larger than the 12.7 km advance ascribed to the Local LGM in northern Peru (Lee et al., 2022).

Moraines set at an intermediate location in the centre of the valleys were likely formed at different phases during the Late Glacial. Phase 4 moraines, including the Hu-IV and Qori Kalis IV moraines, inset of the substantial Phase 1–3 limits, show the separation of the Huancané and Phinaya lobes, with increasing influence of topography.

Phase 5 moraines, such as the Quisoquipina III, Qori Kalis III and Hua-IIIa moraines, show further separation into constituent ice lobes, with the Quisoquipina, Qori Kalis and Huancané lobes all forming distinct, topographically separated lobes (Figure 16). The Phase 5 Hu-IIIa moraines were dated by radiocarbon dating to before 14.2 cal. ka BP

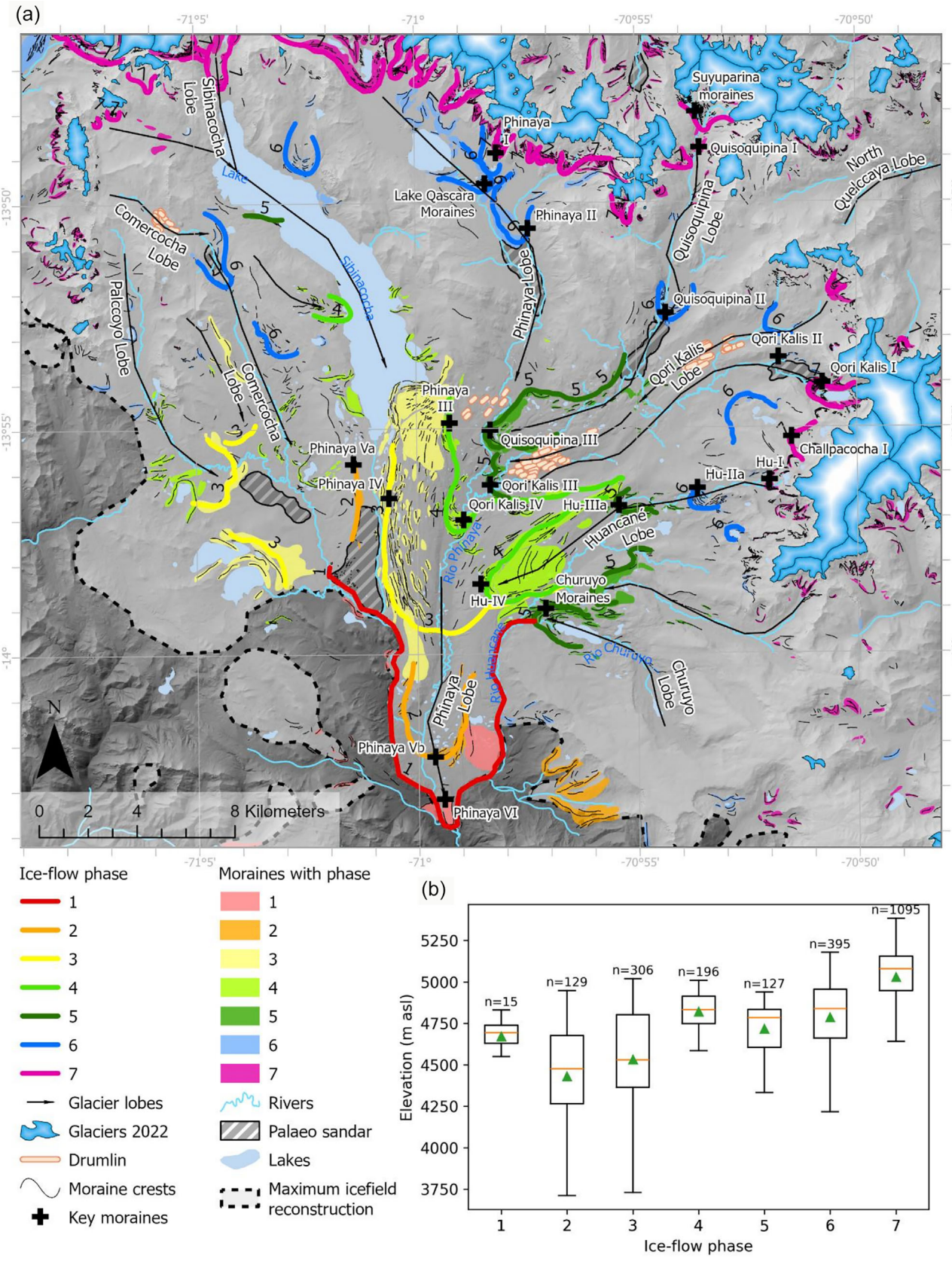

FIGURE 16 A. Reconstruction of ice-flow pathways and morphostratigraphically correlated moraines in Cordillera Vilcanota. Maximum glacier extent (Phase 1) is shown with a black dashed or red line. B. Elevation of each moraine phase from the Sibinacocha Plateau, showing Mean (green triangle) and Median (orange bar) elevation.

(Mercer & Palacios, 1977), and the Hu-IIIb moraines to >13.9 ka by exposure ages (Kelly et al., 2015) (Figure 3). This indicates that they are equivocal with the Antarctic Cold Reversal. An Antarctic Cold Reversal advance in this area is supported by the presence of moraines dating to the Antarctic Cold Reversal in other parts of Peru (Jomelli et al., 2014, 2017).

Phase 6 moraines, including the more ice-distal Quisoquipina II moraines and the more ice-proximal Phinaya II and Lake Qascara

Moraines, occupy a mid to upper-valley position in most lobes. They comprise a series of well-defined, relatively sharp-crested, substantial moraines. Around Quelccaya Ice Cap, some Phase 6 moraines (Hu-IIa) are dated to 11.3 to 12.4 ka (Kelly et al., 2015). Elsewhere in Peru, in Cordillera Blanca, moraines deposited in the Jeullesh Valley (10°S) are also dated to the Younger Dryas Chronozone at 12.4 ka (Glasser et al., 2009b), suggesting a widespread advance at this time. Further, mid-Holocene advances postdating the Younger Dryas are also reported in the Cordillera Vilcabamba (13°20'S) (Licciardi et al., 2009) and Cordillera Blanca (Glasser et al., 2009b). We therefore hypothesise that similarly positioned Phase 6 mid-valley moraines date to the Younger Dryas, and moraines inset of these to the Early Holocene.

Finally, Phase 7 moraines (e.g., Phinaya I, Qori Kalis I, Challpacocha I, Hu-I) are substantial, unvegetated, ice-proximal, sharp-crested and fresh looking with scattered boulders and a silty diamicton matrix. They are the highest-altitude moraines in the study region, with a rise in mean altitude of these features of 450.7 m asl compared with the Phase 1 and 2 moraines that likely predate the gLGM (Figure 16). They have been dated using ^{10}Be exposure ages (Sagredo et al., 2016; Stroup et al., 2015) and lichenometry (Carrivick et al., 2024) to the Late Holocene neoglaciation (0.2–0.5 ka), during the 'Little Ice Age' (Figure 3B). Finally, moraines inset of these limits were formed recently, with abundant moraines forming between ice limits mapped in the RGI (year 2003) and 2022 glacier inventories, some on an annual basis. Further numerical dating is required to test these initial chronological hypotheses.

6 | SUMMARY AND CONCLUSIONS

We investigated the geomorphological imprint of palaeoglacier fluctuations in the Cordillera Vilcanota, high Peruvian Andes. This aims to provide insights into past glacier extent, dynamics and behaviour in an area with sparse geomorphological work. This work, therefore, adds to the currently small body of literature on past glacier behaviour in high, tropical, Andean glaciers. These datasets, in turn, provide reference data for future glacier and climate modelling studies. Chronological work to constrain the numerical exposure ages of the palaeoglacier fluctuations is ongoing. Overall, we mapped ~23,000 features grouped into topographic, glacier, subglacial, ice-marginal, fluvial and lacustrine assemblages, forming one of the most detailed maps of a glacierised tropical mountain range to date. The hydrogeological processes and ways in which these catchment features interact with ground and surface water, including glacier runoff, to support *bofedales* wetland development, are explored in a second, associated publication (Davies et al., submitted).

Widescale geomorphological mapping reveals a landscape heavily dissected by glacial troughs, with lakes frequently forming in the base of the glacial valleys. Moraines formed in the latest Late Holocene neoglacial ('Little Ice Age') are substantial, often enclosing a geomorphological assemblage including flutes, annual moraines and lakes. Beyond these moraines, a series of six further nested moraine sequences documenting past palaeoglacier advances are well preserved across the Sibinacocha Plateau, immediately south of the main ice divide and encircled by the Cordillera Vilcanota icefield and Quelccaya Ice Cap. Within the limits of these moraines is ice-scoured bedrock with roche moutonnées and drumlins, and palaeosandar lie outside moraines. This assemblage indicates temperate palaeoglaciers, with sufficient basal shear stress to deform subglacial sediment. These moraines document a series of glacier stabilisations or advances during the Late Glacial period, likely during both the Antarctic Cold Reversal and Younger Dryas. The largest and stratigraphically oldest moraines reach up to 50 km distant from the ice divide. The reconstructed icefield covers 2,660 km^2, drained by multiple significant and topographically constrained outlet glaciers. This icefield was >70 km across (west–east) and 50 km across (north–south), and was surrounded by multiple and likely independent small cirque and valley glaciers and smaller independent icefields. These outlet ice lobes reached elevations of 3,500 m asl north of the ice divide, but the southerly flowing ice lobes draining across the Sibinacocha Plateau were limited to above 4,500 m asl, which likely reflects the dominant precipitation-bearing wind directions. In the north, the significant Cordillera Vilcanota North Lobe reached 21.5 km from the modern ice divide, with further extension likely limited by rapid altitude decline. The southerly flowing large South Vilcanota Ice Lobe flowed ~35 km across the Sibinacocha Plateau, ice divide to terminus.

AUTHOR CONTRIBUTIONS

BD, TG, OK, TM, JE, NM and JB undertook fieldwork, supported by FD. BD undertook the remotely sensed geomorphological mapping. Funding acquisition: JE, BD, TM, WB, JC. BP and TM provided climatological expertise and data. BD wrote the main manuscript with support from TG and TM. All authors contributed to the manuscript.

ACKNOWLEDGEMENTS

We acknowledge the Natural Environment Research Council grant "Deplete and Retreat: the future of the Andean Water Towers" (NE/X004031/1), awarded to JE, BD, TM and WB. TG was supported by the CENTA doctoral training programme (NE/S007350/1). TanDEM-X (12 m) data were provided by the German Aerospace Center (DLR). We acknowledge the invaluable support of Adrian Ccahuana Condori and Pedro Monarga during fieldwork. Thank you to the local community of Phinaya, who welcomed us and allowed us access to their land.

DATA AVAILABILITY STATEMENT

ESRI Shapefiles are available from the supplementary online information. Hydrological basins are available from Hydrosheds (https://www.hydrosheds.org) (Lehner et al., 2008).

ORCID

Bethan Davies https://orcid.org/0000-0002-8636-1813
Tom Gribbin https://orcid.org/0009-0001-6905-5822
Owen King https://orcid.org/0000-0003-1807-9821
Tom Matthews https://orcid.org/0000-0001-6295-1870
Jan R. Baiker https://orcid.org/0000-0002-2634-0690
Wouter Buytaert https://orcid.org/0000-0001-6994-4454
Jonathan Carrivick https://orcid.org/0000-0002-9286-5348
Fabian Drenkhan https://orcid.org/0000-0002-9443-9596
Juan-Luis García https://orcid.org/0000-0002-9028-7572
Nilton Montoya https://orcid.org/0000-0002-4147-2579
L. Baker Perry https://orcid.org/0000-0003-0598-6393
Jeremy Ely https://orcid.org/0000-0003-4007-1500

REFERENCES

Atkins, C.B. (2013) Geomorphological evidence of cold-based glacier activity in South Victoria Land, Antarctica. *Geological Society, London, Special Publications*, 381(1), 299–318. Available from: https://doi.org/10.1144/SP381.18

Audebaud, E. (1973) Geología de los cuadrángulos de Ocongate y Sicuani 28-t, 29-t-[Boletín A 25].

Bello, C., Suarez, W., Drenkhan, F. & Vega-Jácome, F. (2023) Hydrological impacts of dam regulation for hydropower production: The case of Lake Sibinacocha, Southern Peru. *Journal of Hydrology: Regional Studies*, 46, 101319.

Benn, D.I. (1994) Fabric strength and the interpretation of sedimentary fabric data. *Journal of Sedimentary Research*, A64, 910–915. Available from: https://doi.org/10.1306/D4267F05-2B26-11D7-8648000102C1865D

Benn, D.I. (2004) Clast morphology. In: Evans, D.J.A. & Benn, D.I. (Eds.) *A practical guide to the study of glacial sediments*. London: Arnold, pp. 77–92.

Benn, D.I. (2007) Clast Form Analysis. In: Elias, S.A. (Ed.) *Encyclopedia of Quaternary Science*. Oxford: Elsevier, pp. 904–909.

Benn, D.I. & Ballantyne, C.K. (1993) The description and representation of particle shape. *Earth Surface Processes and Landforms*, 18(7), 665–672. Available from: https://doi.org/10.1002/esp.3290180709

Benn, D.I. & Evans, D.J.A. (2010) *Glaciers & Glaciation*. London: Hodder Education.

Ben-Yehoshua, D., Aradóttir, N., Farnsworth, W.R., Benediktsson, Í.Ö. & Ingólfsson, Ó. (2023) Formation of crevasse-squeeze ridges at Trygghamna, Svalbard. *Earth Surface Processes and Landforms*, 48(12), 2334–2348. Available from: https://doi.org/10.1002/esp.5631

Birkel, S., Mayewski, P., Perry, L., Seimon, A. & Andrade-Flores, M. (2022) Evaluation of reanalysis temperature and precipitation for the Andean Altiplano and Adjacent Cordilleras. *Earth and Space Science*, 9(3), e2021EA001934. Available from: https://doi.org/10.1029/2021EA001934

Bonilla, E.X., Mickley, L.J., Beaudon, E.G., Thompson, L.G., Rodriguez, W.E., Encarnación, R.C., et al. (2023) Contribution of biomass burning to black carbon deposition on Andean glaciers: consequences for radiative forcing. *Environmental Research Letters*, 18(2), 024031. Available from: https://doi.org/10.1088/1748-9326/acb371

Borchers, B., Marrero, S., Balco, G., Caffee, M., Goehring, B., Lifton, N., et al. (2016) Geological calibration of spallation production rates in the CRONUS-Earth project. *Quaternary Geochronology*, 31, 188–198. Available from: https://doi.org/10.1016/j.quageo.2015.01.009

Boston, C.M., Lukas, S. & Carr, S.J. (2015) A Younger Dryas plateau icefield in the Monadhliath, Scotland, and implications for regional palaeoclimate. *Quaternary Science Reviews*, 108, 139–162. Available from: https://doi.org/10.1016/j.quascirev.2014.11.020

Bradley, R.S., Vuille, M., Diaz, H.F. & Vergara, W. (2006) Threats to water supplies in the tropical Andes. *Science*, 312(5781), 1755–1756. Available from: https://doi.org/10.1126/science.1128087

Bradwell, T. (2004) Annual moraines and summer temperatures at Lambatungnajökull, Iceland. *Arctic, Antarctic, and Alpine Research*, 36(4), 502–508. Available from: https://doi.org/10.1657/1523-0430(2004)036[0502:AMASTA]2.0.CO;2

Bromley, G.R.M., Hall, B.L., Schaefer, J.M., Winckler, G., Todd, C.E. & Rademaker, K.M. (2011) Glacier fluctuations in the southern Peruvian Andes during the late-glacial period, constrained with cosmogenic 3He. *Journal of Quaternary Science*, 26(1), 37–43. Available from: https://doi.org/10.1002/jqs.1424

Bromley, G.R.M., Schaefer, J.M., Hall, B.L., Rademaker, K.M., Putnam, A.E., Todd, C.E., et al. (2016) A cosmogenic 10Be chronology for the local last glacial maximum and termination in the Cordillera Oriental, southern Peruvian Andes: Implications for the tropical role in global climate. *Quaternary Science Reviews*, 148, 54–67. Available from: https://doi.org/10.1016/j.quascirev.2016.07.010

Buffen, A.M., Thompson, L.G., Mosley-Thompson, E. & Huh, K.I. (2009) Recently exposed vegetation reveals Holocene changes in the extent of the Quelccaya Ice Cap, Peru. *Quaternary Research*, 72(2), 157–163. Available from: https://doi.org/10.1016/j.yqres.2009.02.007

Bush, M.B., Hansen, B.C.S., Rodbell, D.T., Seltzer, G.O., Young, K.R., León, B., et al. (2005) A 17 000-year history of Andean climate and vegetation change from Laguna de Chochos, Peru. *Journal of Quaternary Science*, 20(7-8), 703–714. Available from: https://doi.org/10.1002/jqs.983

Buytaert, W., Moulds, S., Acosta, L., De Bièvre, B., Olmos, C., Villacis, M., et al. (2017) Glacial melt content of water use in the tropical Andes. *Environmental Research Letters*, 12(11), 114014–114014. Available from: https://doi.org/10.1088/1748-9326/aa926c

Carrivick, J.L., Davies, M., Wilson, R., Davies, B.J., Gribbin, T., King, O., et al. (2024) Accelerating Glacier Area Loss Across the Andes Since the Little Ice Age. *Geophysical Research Letters*, 51(13), e2024GL109154. Available from: https://doi.org/10.1029/2024GL109154

Chandler, B.M.P., Chandler, S.J.P., Evans, D.J.A., et al. (2020) Sub-annual moraine formation at an active temperate Icelandic glacier. *Earth Surface Processes and Landforms*, 45(7), 1622–1643. Available from: https://doi.org/10.1002/esp.4835

Chandler, B.M.P., Lovell, H., Boston, C.M., Lukas, S., Barr, I.D., Benediktsson, Í.Ö., et al. (2018) Glacial geomorphological mapping: A review of approaches and frameworks for best practice. *Earth-Science Reviews*, 185, 806–846. Available from: https://doi.org/10.1016/j.earscirev.2018.07.015

Clark, C.D., Hughes, A.L.C., Greenwood, S.L., Spagnolo, M. & Ng, F.S.L. (2009) Size and shape characteristics of drumlins, derived from a large sample, and associated scaling laws. *Quaternary Science Reviews*, 28(7-8), 677–692. Available from: https://doi.org/10.1016/j.quascirev.2008.08.035

Cordero, R.R., Feron, S., Damiani, A., Sepúlveda, E., Jorquera, J., Redondas, A., et al. (2023) Surface solar extremes in the most irradiated region on earth, Altiplano. *Bulletin of the American Meteorological Society*, 104(6), E1206–E1221. Available from: https://doi.org/10.1175/BAMS-D-22-0215.1

Cuffey, K.M., Conway, H., Hallet, B., Gades, A.M. & Raymond, C.F. (1999) Interfacial water in polar glaciers and glacier sliding at −17°C. *Geophysical Research Letters*, 26(6), 751–754. Available from: https://doi.org/10.1029/1999GL900096

Darvill, C.M., Bentley, M.J., Stokes, C.R. & Shulmeister, J. (2016) The timing and cause of glacial advances in the southern mid-latitudes during the last glacial cycle based on a synthesis of exposure ages from Patagonia and New Zealand. *Quaternary Science Reviews*, 149, 200–214. Available from: https://doi.org/10.1016/j.quascirev.2016.07.024

Davies, B., Bendle, J., Carrivick, J., McNabb, R., McNeil, C., Pelto, M., et al. (2022) Topographic controls on ice flow and recession for Juneau Icefield (Alaska/British Columbia). *Earth Surface Processes and Landforms*, 47(9), 2357–2390. Available from: https://doi.org/10.1002/esp.5383

Davies, B.J., Darvill, C.M., Lovell, H., Bendle, J.M., Dowdeswell, J.A., Fabel, D., et al. (2020) The evolution of the Patagonian Ice Sheet from 35 ka to the present day (PATICE). *Earth-Science Reviews*, 204, 103152. Available from: https://doi.org/10.1016/j.earscirev.2020.103152

Davies, B.J., Gribbin, T., King, O., Matthews, T., Baiker, J., Buytaert, W., et al. submitted. Landsystems of the tropical high Peruvian Andes: glaciers, lakes, wetlands and water resources in Cordillera Vilcanota. *Earth Surface Processes and Landforms*.

Drenkhan, F., Carey, M., Huggel, C., Seidel, J. & Oré, M.T. (2015) The changing water cycle: climatic and socioeconomic drivers of water-related changes in the Andes of Peru. *Wiley Interdisciplinary Reviews: Water*, 2(6), 715–733. https://doi.org/10.1002/wat2.1105

Drenkhan, F., Huggel, C., Guardamino, L. & Haeberli, W. (2019) Managing risks and future options from new lakes in the deglaciating Andes of Peru: The example of the Vilcanota-Urubamba basin. *Science of the Total Environment*, 665, 465–483. Available from: https://doi.org/10.1016/j.scitotenv.2019.02.070

Eaves, S.R., Mackintosh, A.N., Anderson, B.M., Doughty, A.M., Townsend, D.B., Conway, C.E., et al. (2016) The Last Glacial Maximum in the central North Island, New Zealand: palaeoclimate

inferences from glacier modelling. *Climate of the Past*, 12(4), 943–960. Available from: https://doi.org/10.5194/cp-12-943-2016

Ely, J.C., Clark, C.D., Spagnolo, M., Hughes, A.L.C. & Stokes, C.R. (2018) Using the size and position of drumlins to understand how they grow, interact and evolve. *Earth Surface Processes and Landforms*, 43(5), 1073–1087. Available from: https://doi.org/10.1002/esp.4241

Ely, J.C., Clark, C.D., Spagnolo, M., Stokes, C.R., Greenwood, S.L., Hughes, A.L.C., et al. (2016) Do subglacial bedforms comprise a size and shape continuum? *Geomorphology*, 257, 108–119. Available from: https://doi.org/10.1016/j.geomorph.2016.01.001

Ely, J.C., Stevens, D., Clark, C.D. & Butcher, F.E.G. (2023) Numerical modelling of subglacial ribs, drumlins, herringbones, and mega-scale glacial lineations reveals their developmental trajectories and transitions. *Earth Surface Processes and Landforms*, 48(5), 956–978. Available from: https://doi.org/10.1002/esp.5529

Endries, J.L., Perry, L.B., Yuter, S.E., Seimon, A., Andrade-Flores, M., Winkelmann, R., et al. (2018) Radar-Observed Characteristics of Precipitation in the Tropical High Andes of Southern Peru and Bolivia. *Journal of Applied Meteorology and Climatology*, 57(7), 1441–1458. Available from: https://doi.org/10.1175/JAMC-D-17-0248.1

Espinoza, J.C., Garreaud, R., Poveda, G., Arias, P.A., Molina-Carpio, J., Masiokas, M., et al. (2020) Hydroclimate of the Andes Part I: Main Climatic Features. *Frontiers in Earth Science*, 8, 64–64. Available from: https://doi.org/10.3389/feart.2020.00064

Evans, D.J.A. (2013) GLACIAL LANDFORMS|Moraine Forms and Genesis. In: Elias, S.A. & Mock, C.J. (Eds.) *Encyclopedia of Quaternary Science*, Second edition. Amsterdam: Elsevier, pp. 769–779.

Evans, D.J. & Benn, D.I. (2014) *A practical guide to the study of glacial sediments*. London and New York: Routledge.

Evans, D.J. & Benn, D.I. (2021) *A practical guide to the study of glacial sediments*, 2nd edition. London: Quaternary Research Association.

Evans, D.J.A., Ewertowski, M., Roberts, D.H. & Tomczyk, A.M. (2022) The historical emergence of a geometric and sinuous ridge network at the Hørbyebreen polythermal glacier snout, Svalbard and its use in the interpretation of ancient glacial landforms. *Geomorphology*, 406, 108213. Available from: https://doi.org/10.1016/j.geomorph.2022.108213

Evans, D.J.A., Nelson, C.D. & Webb, C. (2010) An assessment of fluting and "till esker" formation on the foreland of Sandfellsjökull, Iceland. *Geomorphology*, 114(3), 453–465. Available from: https://doi.org/10.1016/j.geomorph.2009.08.016

Evans, D.J.A., Strzelecki, M., Milledge, D.G. & Orton, C. (2012) Hørbyebreen polythermal glacial landsystem, Svalbard. *Journal of Maps*, 8(2), 146–156. Available from: https://doi.org/10.1080/17445647.2012.680776

Evans, D.J.A. & Twigg, D.R. (2002) The active temperate glacial landsystem: a model based on Breiethamerkurjokull and Fjallsjokull, Iceland. *Quaternary Science Reviews*, 21(20-22), 2143–2177. Available from: https://doi.org/10.1016/S0277-3791(02)00019-7

Fyffe, C.L., Potter, E., Fugger, S., Orr, A., Fatichi, S., Loarte, E., et al. (2021) The Energy and Mass Balance of Peruvian Glaciers. *Journal of Geophysical Research: Atmospheres*, 126(23), e2021JD034911. Available from: https://doi.org/10.1029/2021JD034911

Gilardoni, S., Di Mauro, B. & Bonasoni, P. (2022) Black carbon, organic carbon, and mineral dust in South American tropical glaciers: A review. *Global and Planetary Change*, 213, 103837. Available from: https://doi.org/10.1016/j.gloplacha.2022.103837

Glasser, N.F. & Bennett, M.R. (2004) Glacial erosional landforms: origins and significance for palaeoglaciology. *Progress in Physical Geography*, 28(1), 43–75. Available from: https://doi.org/10.1191/0309133304pp401ra

Glasser, N.F., Clemmens, S., Schnabel, C., Fenton, C.R. & McHargue, L. (2009) Tropical glacier fluctuations in the Cordillera Blanca, Peru between 12.5 and 7.6 ka from cosmogenic 10Be dating. *Quaternary Science Reviews*, 28(27-28), 3448–3458. Available from: https://doi.org/10.1016/j.quascirev.2009.10.006

Glasser, N.F., Jansson, K.N., Harrison, S. & Kleman, J. (2008) The glacial geomorphology and Pleistocene history of South America between 38°S and 56°S. *Quaternary Science Reviews*, 27(3-4), 365–390. Available from: https://doi.org/10.1016/j.quascirev.2007.11.011

Glasser, N.F., Roman, M., Holt, T.O., Žebre, M., Patton, H. & Hubbard, A.L. (2020) Modification of bedrock surfaces by glacial abrasion and quarrying: Evidence from North Wales. *Geomorphology*, 365, 107283–107283. Available from: https://doi.org/10.1016/j.geomorph.2020.107283

Goodman, A.Y., Rodbell, D.T., Seltzer, G.O. & Mark, B.G. (2001) Subdivision of glacial deposits in southeastern Peru based on pedogenic development and radiometric ages. *Quaternary Research*, 56(1), 31–50. Available from: https://doi.org/10.1006/qres.2001.2221

Gribbin, T., Mackay, J.D., MacDonald, A., Hannah, D.M., Buytaert, W., Baiker, J.R., et al. (2024) Bofedal wetland and glacial melt contributions to dry season streamflow in a high-Andean headwater watershed. *Hydrological Processes*, 38(8), e15237. Available from: https://doi.org/10.1002/hyp.15237

Hall, S.R., Farber, D.L., Ramage, J.M., Rodbell, D.T., Finkel, R.C., Smith, J.A., et al. (2009) Geochronology of Quaternary glaciations from the tropical Cordillera Huayhuash, Peru. *Quaternary Science Reviews*, 28(25-26), 2991–3009. Available from: https://doi.org/10.1016/j.quascirev.2009.08.004

Hughes, P.D., Gibbard, P.L. & Ehlers, J. (2013) Timing of glaciation during the last glacial cycle: evaluating the concept of a global 'Last Glacial Maximum' (LGM). *Earth-Science Reviews*, 125, 171–198. Available from: https://doi.org/10.1016/j.earscirev.2013.07.003

Hugonnet, R., McNabb, R., Berthier, E., Menounos, B., Nuth, C., Girod, L., et al. (2021) Accelerated global glacier mass loss in the early twenty-first century. *Nature*, 592(7856), 726–731. Available from: https://doi.org/10.1038/s41586-021-03436-z

Immerzeel, W., Lutz, A.F., Andrade, M., Bahl, A., Biemans, H., Bolch, T., et al. (2020) Importance and vulnerability of the world's water towers. *Nature*, 577(7790), 364–369. Available from: https://doi.org/10.1038/s41586-019-1822-y

INAIGEM. (2018) El inventario nacional de glaciares: las cordilleras glaciares del Perú.

INAIGEM. (2023) Memoria descriptiva del Inventario Nacional de Glaciares y Laguna de Origen Glaciar del Perú. Dirección de Investigación en Glaciares (DIG) - Instituto Nacional de Investigación en Glaciares y Ecosistemas de Montaña (INAIGEM), Huaraz, Perú.

INGEMMET. (2025) GEOCATMIN - Mapa geológico integrado del Perú a escala 1:50 000 versión ago 2025.

Iturrizaga, L. (2018) Glacial landform assemblages and pedestal moraines in the Cordillera Blanca (Peru). *Geomorphology*, 318, 283–302. Available from: https://doi.org/10.1016/j.geomorph.2018.06.012

Jomelli, V., Favier, V., Vuille, M., Braucher, R., Martin, L., Blard, P.H.H., et al. (2014) A major advance of tropical Andean glaciers during the Antarctic cold reversal. *Nature*, 513(7517), 224–228. Available from: https://doi.org/10.1038/nature13546

Jomelli, V., Khodri, M., Favier, V., Brunstein, D., Ledru, M.-P., Wagnon, P., et al. (2011) Irregular tropical glacier retreat over the Holocene epoch driven by progressive warming. *Nature*, 474(7350), 196–199. Available from: https://doi.org/10.1038/nature10150

Jomelli, V., Martin, L., Blard, P.H., Favier, V., Vuillé, M. & Ceballos, J.L. (2017) Revisiting the Andean tropical glacier behavior during the Antarctic Cold Reversal. *Cuadernos de Investigación Geográfica*, 43(2), 629–648. Available from: https://doi.org/10.18172/cig.3201

Jónsson, S.A., Benediktsson, Í.Ö., Ingólfsson, Ó., Schomacker, A., Bergsdóttir, H.L., Jacobson, W.R., et al. (2016) Submarginal drumlin formation and late Holocene history of Fláajökull, southeast Iceland. *Annals of Glaciology*, 57(72), 128–141. Available from: https://doi.org/10.1017/aog.2016.4

Junquas, C., Takahashi, K., Condom, T., Espinoza, J.C., Chavez, S., Sicart, J.E., et al. (2018) Understanding the influence of orography on the precipitation diurnal cycle and the associated atmospheric processes in the central Andes. *Climate Dynamics*, 50(11-12), 3995–4017. Available from: https://doi.org/10.1007/s00382-017-3858-8

Kelly, M.A., Lowell, T.V., Applegate, P.J., Phillips, F.M., Schaefer, J.M., Smith, C.A., et al. (2015) A locally calibrated, late glacial 10Be production rate from a low-latitude, high-altitude site in the Peruvian Andes. *Quaternary Geochronology*, 26, 70–85. Available from: https://doi.org/10.1016/j.quageo.2013.10.007

Kochtitzky, W.H., Edwards, B.R., Enderlin, E.M., Marino, J. & Marinque, N. (2018) Improved estimates of glacier change rates at Nevado Coropuna Ice Cap, Peru. *Journal of Glaciology*, 64(244), 175–184. Available from: https://doi.org/10.1017/jog.2018.2

Kronenberg, M., Schauwecker, S., Huggel, C., Salzmann, N., Drenkhan, F., Frey, H., et al. (2016) The Projected Precipitation Reduction over the Central Andes may Severely Affect Peruvian Glaciers and Hydropower Production. *Energy Procedia*, 97, 270–277. Available from: https://doi.org/10.1016/j.egypro.2016.10.072

Le Heron, D.P., Kettler, C., Davies, B.J., Scharfenberg, L., Eder, L., Ketterman, M., et al. (2021) Rapid geomorphological and sedimentological changes at a modern Alpine ice margin: lessons from the Gepatsch Glacier, Tirol, Austria. *Journal of the Geological Society*, 179(3), jgs2021-2052. Available from: https://doi.org/10.1144/jgs2021-052

Le Heron, D.P., Vandyk, T.M., Kuang, H., Liu, Y., Chen, X., Wang, Y., et al. (2019) Bird's-eye view of an Ediacaran subglacial landscape. *Geology*, 47(8), 705–709. Available from: https://doi.org/10.1130/G46285.1

Lee, E., Ross, N., Henderson, A.C.G., Russell, A.J., Jamieson, S.S.R. & Fabel, D. (2022) Palaeoglaciation in the Low Latitude, Low Elevation Tropical Andes, Northern Peru. *Frontiers in Earth Science*, 10, 838826. Available from: https://doi.org/10.3389/feart.2022.838826

Leger, T.P.M., Hein, A.S., Bingham, R.G., Martini, M.A., Soteres, R.L., Sagredo, E.A., et al. (2020) The glacial geomorphology of the Río Corcovado, Río Huemul and Lago Palena/General Vintter valleys, northeastern Patagonia (43°S, 71°W). *Journal of Maps*, 16(2), 651–668. Available from: https://doi.org/10.1080/17445647.2020.1794990

Lehner, B., Verdin, K. & Jarvis, A. (2008) New global hydrography derived from spaceborne elevation data. *Eos, Transactions American Geophysical Union*, 89(10), 93–94. Available from: https://doi.org/10.1029/2008EO100001

Licciardi, J.M., Schaefer, J.M., Taggart, J.R. & Lund, D.C. (2009) Holocene glacier fluctuations in the Peruvian Andes indicate northern climate linkages. *Science*, 325(5948), 1677–1679. Available from: https://doi.org/10.1126/science.1175010

Lifton, N., Sato, T. & Dunai, T.J. (2014) Scaling in situ cosmogenic nuclide production rates using analytical approximations to atmospheric cosmic-ray fluxes. *Earth and Planetary Science Letters*, 386, 149–160. Available from: https://doi.org/10.1016/j.epsl.2013.10.052

Lorrain, R.D. & Fitzsimons, S.J. (2011) Cold-Based Glaciers. In: Singh, V.P., Singh, P. & Haritashya, U.K. (Eds.) *Encyclopedia of Snow, Ice and Glaciers*. Netherlands, Dordrecht: Springer, pp. 157–161.

Lukas, S. (2006) Morphostratigraphic principles in glacier reconstruction - a perspective from the British Younger Dryas. *Progress in Physical Geography*, 30(6), 719–736. Available from: https://doi.org/10.1177/0309133306071955

Lukas, S., Benn, D.I., Boston, C.M., Brook, M., Coray, S., Evans, D.J.A., et al. (2013) Clast shape analysis and clast transport paths in glacial environments: A critical review of methods and the role of lithology. *Earth-Science Reviews*, 121, 96–116. Available from: https://doi.org/10.1016/j.earscirev.2013.02.005

Małecki, J., Lovell, H., Ewertowski, W., Górski, Ł., Kurczaba, T., Latos, B., et al. (2018) The glacial landsystem of a tropical glacier: Charquini Sur, Bolivian Andes. *Earth Surface Processes and Landforms*, 43(12), 2584–2602. Available from: https://doi.org/10.1002/esp.4417

Mark, B.G., Seltzer, G.O., Rodbell, D.T. & Goodman, A.Y. (2002) Rates of deglaciation during the last glaciation and Holocene in the Cordillera Vilcanota-Quelccaya Ice Cap region, southeastern Peru. *Quaternary Research*, 57(3), 287–298. Available from: https://doi.org/10.1006/qres.2002.2320

Mark, B., Stansell, N. & Zeballos, G. (2017) The last deglaciation of Peru and Bolivia. Cuadernos de investigación geográfica. *Geographical Research Letters*, 43(2), 591–628. Available from: https://doi.org/10.18172/cig.3265

Martin, J.R.V., Davies, B.J. & Thorndycraft, V.R. (2019) Glacier dynamics during a phase of Late Quaternary warming in Patagonia reconstructed from sediment-landform associations. *Geomorphology*, 337, 111–133. Available from: https://doi.org/10.1016/j.geomorph.2019.03.007

McCerery, R., Davies, B.J., Lovell, H., Pearce, D.A., Calvo-Ryan, R., Małecki, J., et al. (2024) Terrestrial glacial geomorphology of surge-type and non-surge-type glaciers on Svalbard. *Journal of Maps*, 20(1), 2362277. Available from: https://doi.org/10.1080/17445647.2024.2362277

Mercer, J.H. & Palacios, M.O. (1977) Radiocarbon dating of the last glaciation in Peru. *Geology*, 5(10), 600–604. Available from: https://doi.org/10.1130/0091-7613(1977)5<600:RDOTLG>2.0.CO;2

Millan, R., Mouginot, J., Rabatel, A. & Morlighem, M. (2022) Ice velocity and thickness of the world's glaciers. *Nature Geoscience*, 15(2), 124–129. Available from: https://doi.org/10.1038/s41561-021-00885-z

Muñoz, R., Vaghefi, S., Drenkhan, F., Santos, M., Viviroli, D., Muccione, V., et al. (2024) Assessing Water Management Strategies in Data-Scarce Mountain Regions under Uncertain Climate and Socio-Economic Changes. *Water Resources Management*, 38, 1–18. Available from: https://doi.org/10.1007/s11269-024-03853-5

Narro Pérez, R.A., Eyles, C.H., Lee, R.E., Dàvila Röller, L. & Maclachlan, J.C. (2023) Landsystem analysis of a tropical moraine-dammed supraglacial lake, Llaca Lake, Cordillera Blanca, Perú. *Boreas*, 52(2), 272–293. Available from: https://doi.org/10.1111/bor.12611

Palacios, D., Stokes, C.R., Phillips, F.M., Clague, J.J., Alcalá-Reygosa, J., Andres, N., et al. (2020) The deglaciation of the Americas during the Last Glacial Termination. *Earth-Science Reviews*, 203, 103113–103113. Available from: https://doi.org/10.1016/j.earscirev.2020.103113

Pall, I.A., Meraj, G. & Romshoo, S.A. (2019) Applying integrated remote sensing and field-based approach to map glacial landform features of the Machoi Glacier valley, NW Himalaya. *SN Applied Sciences*, 1(5), 488. Available from: https://doi.org/10.1007/s42452-019-0503-7

Pedro, J.B., Bostock, H.C., Bitz, C.M., He, F., Vandergoes, M.J., Steig, E.J., et al. (2016) The spatial extent and dynamics of the Antarctic Cold Reversal. *Nature Geoscience*, 9(1), 51–55. Available from: https://doi.org/10.1038/ngeo2580

Perry, L.B., Seimon, A., Andrade-Flores, M.F., Endries, J.L., Yuter, S.E., Velarde, F., et al. (2017) Characteristics of Precipitating Storms in Glacierized Tropical Andean Cordilleras of Peru and Bolivia. *Annals of the American Association of Geographers*, 107(2), 309–322. Available from: https://doi.org/10.1080/24694452.2016.1260439

Perry, L.B., Seimon, A. & Kelly Ginger, M. (2014) Precipitation delivery in the tropical high Andes of southern Peru: new findings and paleoclimatic implications. *International Journal of Climatology*, 34(1), 197–215. Available from: https://doi.org/10.1002/joc.3679

Powers, M.C. (1953) A new roundness scale for sedimentary particles. *Journal of Sedimentary Petrology*, 23, 117–119. Available from: https://doi.org/10.1306/D4269567-2B26-11D7-8648000102C1865D

Rabatel, A., Machaca, A., Francou, B. & Jomelli, V. (2006) Glacier recession on Cerro Charquini (16 S), Bolivia, since the maximum of the Little Ice Age (17th century). *Journal of Glaciology*, 52(176), 110–118. Available from: https://doi.org/10.3189/172756506781828917

Randolph Glacier Inventory Consortium, Arendt, A., Bliss, A., Bolch, T., Cogley, J.G., Gardner, A., et al. (2017) Randolph glacier inventory–a dataset of global glacier outlines: Version 6.0: technical report, Digital Media. RGI Consortium, Colorado, USA.

Rasmussen, S.O., Andersen, K.K., Svensson, A.M., Steffensen, J.P., Vinther, B.M., Clausen, H.B., et al. (2006) A new Greenland ice core chronology for the last glacial termination. *Journal of Geophysical Research: Atmospheres*, 111(D6), D06102. Available from: https://doi.org/10.1029/2005JD006079

Reimer, P.J., Austin, W.E.N., Bard, E., Bayliss, A., Blackwell, P.G., Bronk Ramsey, C., et al. (2020) THE INTCAL20 NORTHERN HEMISPHERE

RADIOCARBON AGE CALIBRATION CURVE (0–55 CAL kBP). *Radiocarbon*, 62(4), 1–33. Available from: https://doi.org/10.1017/RDC.2020.41

RGI 7.0 Consortium. (2023) Randolph Glacier Inventory - A Dataset of Global Glacier Outlines, Version 7.0, in: Center, N.N.S.a.I.D. (Ed.), Boulder, Colorado USA.

Rivers, G.E., Storrar, R.D., Jones, A.H. & Ojala, A.E.K. (2023) 3D morphometry of De Geer Moraines and Crevasse-Squeeze Ridges: Differentiating between pushing and squeezing mechanisms from remotely sensed data. *Quaternary Science Reviews*, 321, 108383. Available from: https://doi.org/10.1016/j.quascirev.2023.108383

Roberson, S., Hubbard, B., Coulson, H.R. & Boomer, I. (2011) Physical properties and formation of flutes at a polythermal valley glacier: midre lovénbreen, svalbard. *Geografiska Annaler: Series A, Physical Geography*, 93(2), 71–88. Available from: https://doi.org/10.1111/j.1468-0459.2011.00420.x

Roberts, D.H. & Long, A.J. (2005) Streamlined bedrock terrain and fast ice flow, Jakobshavns Isbrae, West Greenland: implications for ice stream and ice sheet dynamics. *Boreas*, 34(1), 25–42. Available from: https://doi.org/10.1080/03009480510012818

Rodbell, D.T., Hatfield, R.G., Abbott, M.B., Chen, C.Y., Woods, A., Stoner, J.S., et al. (2022) 700,000 years of tropical Andean glaciation. *Nature*, 607(7918), 301–306. Available from: https://doi.org/10.1038/s41586-022-04873-0

Sagredo, E.A. & Lowell, T.V. (2012) Climatology of Andean glaciers: A framework to understand glacier response to climate change. *Global and Planetary Change*, 86, 101–109. Available from: https://doi.org/10.1016/j.gloplacha.2012.02.010

Sagredo, E.A., Lowell, T.V., Kelly, M.A., Rupper, S., Aravena, J.C., Ward, D.J., et al. (2016) Equilibrium line altitudes along the Andes during the Last millennium: Paleoclimatic implications. *The Holocene*, 27(7), 1019–1033. Available from: https://doi.org/10.1177/0959683616678458

Saha, S., Sharma, M.C., Murari, M.K., Owen, L.A. & Caffee, M.W. (2016) Geomorphology, sedimentology and minimum exposure ages of streamlined subglacial landforms in the NW Himalaya, India. *Boreas*, 45(2), 284–303. Available from: https://doi.org/10.1111/bor.12153

Salzmann, N., Huggel, C., Rohrer, M., Silverio, W., Mark, B.G., Burns, P., et al. (2013) Glacier changes and climate trends derived from multiple sources in the data scarce Cordillera Vilcanota region, southern Peruvian Andes. *The Cryosphere*, 7(1), 103–118. Available from: https://doi.org/10.5194/tc-7-103-2013

Schauwecker, S., Rohrer, M., Acuña, D., Cochachin, A., Dávila, L., Frey, H., et al. (2014) Climate trends and glacier retreat in the Cordillera Blanca, Peru, revisited. *Global and Planetary Change*, 119, 85–97. Available from: https://doi.org/10.1016/j.gloplacha.2014.05.005

Schauwecker, S., Rohrer, M., Huggel, C., Endries, J., Montoya, N., Neukom, R., et al. (2017) The freezing level in the tropical Andes, Peru: An indicator for present and future glacier extents. *Journal of Geophysical Research: Atmospheres*, 122(10), 5172–5189. Available from: https://doi.org/10.1002/2016JD025943

Shakun, J.D., Clark, P.U., Marcott, S.A., Brook, E.J., Lifton, N.A., Caffee, M., et al. (2015) Cosmogenic dating of Late Pleistocene glaciation, southern tropical Andes, Peru. *Journal of Quaternary Science*, 30(8), 841–847. Available from: https://doi.org/10.1002/jqs.2822

Sharp, M. (1985) "Crevasse-Fill" Ridges—A Landform Type Characteristic of Surging Glaciers? *Geografiska Annaler: Series A, Physical Geography*, 67(3-4), 213–220. Available from: https://doi.org/10.1080/04353676.1985.11880147

Smith, J.A., Seltzer, G.O., Farber, D.L., Rodbell, D.T. & Finkel, R.C. (2005a) Early Local Last Glacial Maximum in the Tropical Andes. *Science*, 308(5722), 678–681. Available from: https://doi.org/10.1126/science.1107075

Smith, J.A., Seltzer, G.O., Rodbell, D.T. & Klein, A.G. (2005b) Regional synthesis of last glacial maximum snowlines in the tropical Andes, South America. *Quaternary International*, 138-139, 145–167. Available from: https://doi.org/10.1016/j.quaint.2005.02.011

Sneed, E.D. & Folk, R.L. (1958) Pebbles in the Lower Colorado River, Texas a Study in Particle Morphogenesis. *The Journal of Geology*, 66(2), 114–150. Available from: https://doi.org/10.1086/626490

Soruco, A., Vincent, C., Rabatel, A., Francou, B., Thibert, E., Sicart, J.E., et al. (2015) Contribution of glacier runoff to water resources of La Paz city, Bolivia (16 S). *Annals of Glaciology*, 56(70), 147–154. Available from: https://doi.org/10.3189/2015AoG70A001

Spagnolo, M., Clark, C.D., Hughes, A.L., Dunlop, P. & Stokes, C.R. (2010) The planar shape of drumlins. *Sedimentary Geology*, 232(3-4), 119–129. Available from: https://doi.org/10.1016/j.sedgeo.2010.01.008

Stokes, C.R., Fowler, A.C., Clark, C.D., Hindmarsh, R.C.A. & Spagnolo, M. (2013) The instability theory of drumlin formation and its explanation of their varied composition and internal structure. *Quaternary Science Reviews*, 62, 77–96. Available from: https://doi.org/10.1016/j.quascirev.2012.11.011

Stroup, J.S., Kelly, M.A., Lowell, T.V., Applegate, P.J. & Howley, J.A. (2014) Late Holocene fluctuations of Qori Kalis outlet glacier, Quelccaya Ice Cap, Peruvian Andes. *Geology*, 42(4), 347–350. Available from: https://doi.org/10.1130/G35245.1

Stroup, J.S., Kelly, M.A., Lowell, T.V., Smith, C.A., Beal, S.A., Landis, J.D., et al. (2015) Late Holocene fluctuations of Quelccaya Ice Cap, Peru, registered by nearby lake sediments. *Journal of Quaternary Science*, 30(8), 830–840. Available from: https://doi.org/10.1002/jqs.2821

Stuiver, M. & Reimer, P.J. (1993) Extended 14C data base and revised CALIB 3.0 14C age calibration program. *Radiocarbon*, 35(1), 215–230. Available from: https://doi.org/10.1017/S0033822200013904

Taylor, L.S., Quincey, D.J., Smith, M.W., Potter, E.R., Castro, J. & Fyffe, C.L. (2022) Multi-Decadal Glacier Area and Mass Balance Change in the Southern Peruvian Andes. *Frontiers in Earth Science*, 10, 863933. Available from: https://doi.org/10.3389/feart.2022.863933

Thompson, L.G. (2000) Ice core evidence for climate change in the Tropics: implications for our future. *Quaternary Science Reviews*, 19(1-5), 19–35. Available from: https://doi.org/10.1016/S0277-3791(99)00052-9

Thompson, L.G., Mosley-Thompson, E., Brecher, H., Davis, M., León, B., Les, D., et al. (2006) Abrupt tropical climate change: Past and present. *PNAS*, 103(28), 10536–10543. Available from: https://doi.org/10.1073/pnas.0603900103

Thompson, L.G., Mosley-Thompson, E., Davis, M.E. & Porter, S.E. (2017) Ice core records of climate and environmental variability in the Tropical Andes of Peru: past present and future. *Revista de Glaciares y ecosistemas de montaña*, 3, 25–40.

Thompson, L.G., Mosley-Thompson, E., Davis, M.E., Zagorodnov, V.S., Howat, I.M., Mikhalenko, V.N., et al. (2013) Annually resolved ice core records of tropical climate variability over the past∼ 1800 years. *Science*, 340(6135), 945–950. Available from: https://doi.org/10.1126/science.1234210

Vergara, W., Deeb, A., Valencia, A., Bradley, R., Francou, B., Zarzar, A., et al. (2007) Economic impacts of rapid glacier retreat in the Andes. *Eos, Transactions American Geophysical Union*, 88(25), 261–264. Available from: https://doi.org/10.1029/2007EO250001

Vickers, A.C., Shakun, J.D., Goehring, B.M., Gorin, A., Kelly, M.A., Jackson, M.S., et al. (2021) Similar Holocene glaciation histories in tropical South America and Africa. *Geology*, 49(2), 140–144. Available from: https://doi.org/10.1130/G48059.1

Wanner, H., Pfister, C. & Neukom, R. (2022) The variable European Little Ice Age. *Quaternary Science Reviews*, 287, 107531. Available from: https://doi.org/10.1016/j.quascirev.2022.107531

Weng, C., Bush, M.B., Curtis, J.H., Kolata, A.L., Dillehay, T.D. & Binford, M.W. (2006) Deglaciation and Holocene climate change in the western Peruvian Andes. *Quaternary Research*, 66(1), 87–96. Available from: https://doi.org/10.1016/j.yqres.2006.01.004

Wood, J.L., Harrison, S., Wilson, R., Emmer, A., Yarleque, C., Glasser, N.F., et al. (2021) Contemporary glacial lakes in the Peruvian Andes. *Global and Planetary Change*, 204, 103574. Available from: https://doi.org/10.1016/j.gloplacha.2021.103574

Zech, R., Smith, J., Kaplan, M.R. (2009) Chronologies of the Last Glacial Maximum and its Termination in the Andes (∼ 10–55° S) based on surface exposure dating, *Past Climate Variability in South America and Surrounding Regions: From the Last Glacial Maximum to the Holocene*, pp. 61-87.

Zhao, B., Russell, J.M., Blaus, A., Nascimento, M.D., Freeman, A. & Bush, M.B. (2024) Tropical Andean climate variations since the last deglaciation. *Proceedings of the National Academy of Sciences*, 121(34), e2320143121. Available from: https://doi.org/10.1073/pnas.2320143121

SUPPORTING INFORMATION

Additional supporting information can be found online in the Supporting Information section at the end of this article.

How to cite this article: Davies, B., Gribbin, T., King, O., Matthews, T., Baiker, J.R., Buytaert, W. et al. (2026) Palaeoglacier reconstruction and dynamics of Cordillera Vilcanota in the tropical high Peruvian Andes. *Earth Surface Processes and Landforms*, 51(2), e70246. Available from: https://doi.org/10.1002/esp.70246